Late Cenozoic and modern stress fields in the wester Fars (Iran) : Implications for the tectonic and kinematic evolution of Central Zagros

Olivier Lacombe, Frédéric Mouthereau, S. Kargar, Bertrand Meyer

Late Cenozoic and modern stress fields in the western Fars (Iran): Implications for the tectonic and kinematic evolution of central Zagros

O. Lacombe and F. Mouthereau

Laboratoire de Tectonique, UMR 7072 CNRS, Université Pierre et Marie Curie, Paris, France

S. Kargar

Geological Survey of Iran, Shiraz, Iran

B. Meyer

Laboratoire de Tectonique, UMR 7072 CNRS, Université Pierre et Marie Curie, Paris, France

Received 11 April 2005; revised 23 September 2005; accepted 28 October 2005; published 21 January 2006.

[1] The Zagros (Iran) developed during Mio-Pliocene times in response to Arabia-Eurasia convergence. The western Fars highlights a major bend of the deformation front and displays a remarkable set of nearly N-S right-lateral strike-slip faults (the Kazerun-Borazjan/Karebass/Sabz-Pushan/Sarvestan faults) oblique at high angle to the belt. The region likely plays a major kinematic role by accommodating the change in shortening modes from partitioned in the western central Zagros to nonpartitioned in the eastern Zagros. The inversion of focal mechanisms from small and moderate earthquakes shows a consistent N020°–030° compression with a low ratio between differential stresses. This regime accounts for the combination of strike-slip and thrust-type mechanisms through likely σ2/σ3 permutations. Fault slip analysis reveals two successive late Cenozoic regional compressional trends, NE-SW then N020°. The latter is in good agreement with the present-day stress. The significance of the NE-SW compression is discussed alternatively in terms of stress deviations or block rotations in relation to the strike-slip fault system. Fieldwork and satellite imagery suggest that these faults behave first as transfer faults during folding of the cover and later as strike-slip faults, in agreement with the succession of stress regimes and the evolution of the dominant deformation style from thin-skinned to thick-skinned. The first-order stability of the collision-related state of stress since ~5 Ma supports that the Arabia-Eurasia convergence did not give rise to partitioning in the western Fars but rather was (and is still) accommodated by distributed deformation involving both shortening and strike-slip motion throughout the cover and the basement. **Citation:** Lacombe, O., F. Mouthereau, S. Kargar, and B. Meyer (2006), Late Cenozoic and modern stress fields in the western Fars (Iran): Implications for the tectonic and kinematic evolution of central Zagros, *Tectonics*, *25*, TC1003, doi:10.1029/2005TC001831.

0278-7407/06/2005TC001831$12.00

1. Introduction and Scope of the Study

[2] Iran is located within the active convergence zone between the Arabian and Eurasian plates (Figure 1). The pole of the rotation is located near the Libyan coast [*McClusky et al.*, 2000, 2003; *Vernant et al.*, 2004], and the convergence velocity increases from the Bitlis collision zone to the Makran. In Iran, the Arabia-Eurasia convergence is trending N-S to NNE. Estimates of its velocity range from 22 mm yr^{-1} [*Bayer et al.*, 2002] to 35 mm yr^{-1} [*DeMets et al.*, 1990] (Figure 1a). The most reliable convergence vector is provided by recent GPS studies at the Arabian plate scale and corresponds to a velocity of about 22–25 mm yr^{-1} in a N010°E direction at the longitude 56°E [*McClusky et al.*, 2003; *Vernant et al.*, 2004] (Figure 1a).

[3] The Main Zagros Thrust (MZT) is the geological boundary between the Iranian Plateau to the north and the Zagros fold belt to the south (Figure 2). It corresponds to the suture, currently inactive, between the colliding plates of central Iran and the Arabian passive continental margin [*Berberian*, 1995]. The Zagros belt developed mainly as a result of folding (and thrusting) of the Cenozoic foreland sequence and the underlying Paleozoic-Mesozoic deposits of the Arabian margin and platform. The belt is divided into several zones that differ according to their structural style and sedimentary history [*Stocklin*, 1968, 1974; *Falcon*, 1974; *Berberian and King*, 1981; *Motiei*, 1993]; from west to east, the Lorestan salient, the Dezful recess, and the Fars salient (Figure 2) reflect and underline this along-strike structural and kinematic segmentation. Farther east, the Minab-Zendan transpressional fault system [e.g., *Regard et al.*, 2004] accommodates the transition from the Zagros collisional belt to the Makran subduction accretionary wedge.

[4] The investigated area covers the western part of the Fars, where a major bend of the deformation front and fold axes occurs (Figures 2 and 3). On the structural point of view, this area is marked by a remarkable set of four

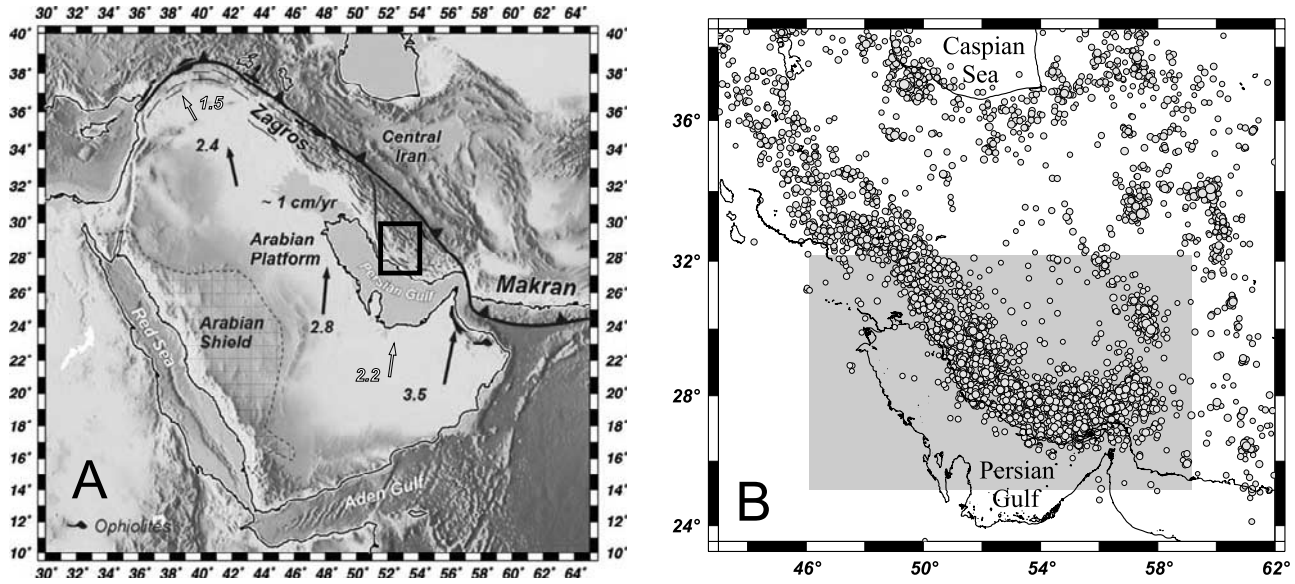

Figure 1. (a) Geodynamic setting of the Arabia-Eurasia collision. Arabia-Eurasia convergence vectors after NUVEL-1 [*DeMets et al.*, 1990] (black) and GPS studies [*Vernant et al.*, 2004] (white). Velocities in cm/yr. (b) Seismicity in Iran between 1964 and 2002. There were 4501 events recorded, $2.4 < m_b < 7.4$ (from International Seismological Centre, online bulletin, available at http://www.isc.ac.uk/Bull, Thatcham, U.K., 2001).

N-S to N150° right-lateral strike-slip faults (the Kazerun-Borazjan/Karebass/Sabz-Pushan/Sarvestan faults, Figure 3b) cutting across the structural grain of the belt and terminating as thrusts parallel to the folds. This particular area is thought to play a major kinematic role by accommodating the change in shortening modes from the western central Zagros to the eastern Zagros. While in the western central Zagros the Arabia-Eurasia convergence is currently partitioned into

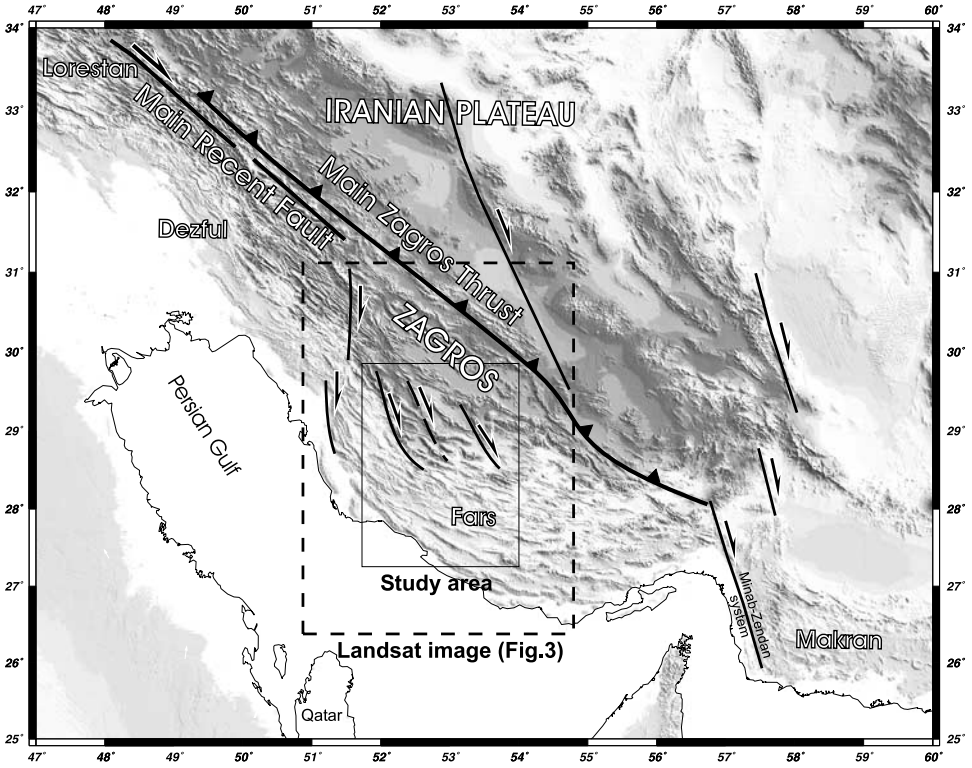

Figure 2. Topography (GTOPO30) and main structural features of the SE part of the Zagros belt.

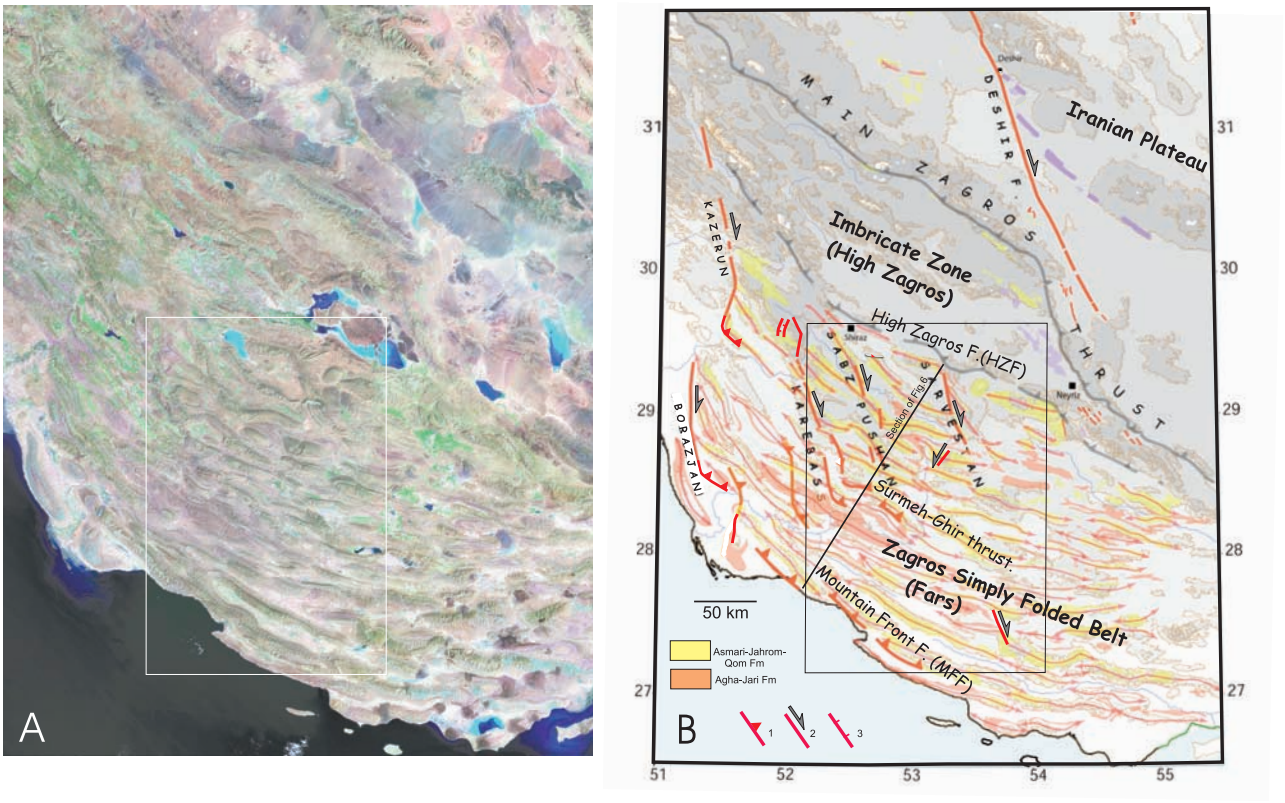

Figure 3. (a) Landsat TM image and (b) schematic structural map of the Fars. Topographic contours (GTOPO30) and shading every 500 m. The main anticline axes have been reported. Areas have been highlighted where the syntectonic Agha Jari Formation and the Oligo-(Miocene) Asmari-Jahrom/Qom formations crop out; 1, thrust; 2, strike-slip fault; 3, normal fault.

NE-SW shortening perpendicular to the belt and right-lateral strike-slip faulting along the Main Recent Fault (MRF), deformation in the eastern Zagros (Fars) involves shortening parallel to convergence which is perpendicular to the local nearly E-W trend of the belt [*Talebian and Jackson*, 2004]. This kinematic change requires extension along the strike of the belt, which can be achieved by the Kazerun-Borazjan/Karebass/Sabz-Pushan/Sarvestan faults (Figure 3) if they rotate anticlockwise about vertical axes [*Talebian and Jackson*, 2004]. This fault system has been alternatively discussed as an orogen-scale horse-tail strike-slip fault termination which transfers and distributes orogen-parallel dextral slip achieved along the MRF into the thrusts and folds of the Zagros belt [*Authemayou et al.*, 2005]. The western Fars is therefore a key region to understand the late Cenozoic tectonic and kinematic evolution of the Zagros belt including the past and current configuration of faulting. The purpose of this paper is to provide constraints on this evolution through an analysis of the geometry and the kinematics of folds and strike-slip faults in relation to the late Cenozoic and modern stress regimes. Special attention has been paid to the tectonic behavior and the geological evolution of the strike-slip faults. Hence we carried out a structural analysis of the tectonic features of the western Fars region combining fieldwork, morphostructural studies and tectonic analyses based on inversion of fault slip data and earthquake focal mechanisms.

2. Geological Setting of the Fars Area

2.1. Structural Setting

[5] The Zagros is a folded belt within the Arabian plate with an overall NW-SE strike evolving to ENE-WSW in its SE part (Figure 2). The transversal NE trending shortening rate increases from NW to SE and reaches about 10 mm yr^{-1} near its SE edge [*Tatar et al.*, 2002; *Vernant et al.*, 2004]. The fold-and-thrust belt affects a roughly 6–15 km thick sedimentary pile that overlies a Precambrian metamorphic basement corresponding to the rifted Arabian shield [*McCall*, 1997].

[6] The Fars region is limited to the west from the Dezful by the Kazerun-Borazjan Fault (KBF), a seismically active major right-lateral strike-slip fault [*Baker et al.*, 1993; *Bachmanov et al.*, 2004; *Authemayou et al.*, 2005; *Sepehr and Cosgrove*, 2005]. This fault crosses the Zagros trend and is associated with bends and right-lateral offsets of fold axes (Figure 3). West of the KBF the width of the belt is narrow, the Hormuz salt is generally absent (it is, however, present north of the Izeh zone) and earthquakes appear localized along major thrusts [*Berberian*, 1995]; to

the east the earthquakes are distributed over the entire belt and the Hormuz salt is the master decollement. South of the MZT, the high Zagros (or the imbricate zone) consists of a highly faulted thrust belt with a NW-SE trend. This belt is bounded to the SW by the High Zagros Fault (HZF) and is upthrusted onto the northern part of the Simply Folded Belt. The Simply Folded Belt (SFB) is limited to the SW by the Mountain Front Fault (MFF) (Figure 3), a master segmented blind thrust with striking structural, topographic and seismotectonic characteristics [*Berberian*, 1995].

[7] The pattern of deformation of the cover and its variation along the strike of the belt highly depend on the occurrence of potential decollement levels [e.g., *O'Brien*, 1957]. In the Fars, fault/folds systems within the sedimentary cover generally detach on the Hormuz salt [*Colman-Sadd*, 1978]. The thickness of this formation, estimated about 1–2 km in the Fars region, played a significant role in the cover-basement decoupling. The low taper angle, the great width and the arcuate shape in map view of the Zagros fold belt in the Fars region are commonly considered as reflecting thin-skinned deformation [e.g., *Cotton and Koyi*, 2000; *Costa and Vendeville*, 2002; *Bahroudi and Koyi*, 2003]. The lithology of the potential decollement levels, the variation in thickness of the sedimentary sequence and the predeformational basin geometry likely controlled the differential propagation of the thrust belt segments toward the foreland [*Macedo and Marshak*, 1999; *Letouzey et al.*, 2002; *McQuarrie*, 2004; S. Sherkati et al., The central Zagros fold-thrust belt (Iran): New insights from seismic data, field observations and sandbox modeling, submitted to *Tectonics*, 2005, hereinafter referred to as Sherkati et al., submitted manuscript, 2005), leading to the succession of salients (Lorestan, Fars) and recesses (Dezful). Accordingly, the thick salt at the base of the sedimentary cover in the Fars has resulted in a relatively far propagation of the deformation front toward the SW; the KBF has decoupled the deformation in the Fars from that in the Dezful Embayment to the west (Figure 2) where the Hormuz salt is absent. For these reasons, until recently most authors have considered the deformation of the SFB to be essentially of thin-skinned type above Paleozoic detachment levels [e.g., *Cotton and Koyi*, 2000; *McQuarrie*, 2004].

[8] Reactivated basement normal faults at a depth of between 10 and 20 km are however thought for a long time to be responsible for the major earthquakes along the Zagros belt [*Berberian and King*, 1981; *Berberian*, 1995; *Jackson*, 1980; *Jackson and Fitch*, 1981; *Jackson and McKenzie*, 1984]. Basement structures likely played a role in the deformation of the Zagros by localizing some topographic steps and major (often active) thrust faults in the cover [*Berberian*, 1995; *Letouzey et al.*, 2002; *Mouthereau et al.*, 2005]. Recent balanced cross sections in the westernmost and easternmost Fars clearly emphasize that the basement is involved in shortening [*Letouzey and Sherkati*, 2004; *Molinaro et al.*, 2005; Sherkati et al., submitted manuscript, 2005]. Recent critical wedge modeling [*Mouthereau et al.*, 2005] suggests that thin-skinned tectonics does not account for the regional topography of the Fars and that deformation and topography of this area are mainly controlled by basement-involved shortening.

2.2. Sedimentary Setting

[9] After the Permo-Triassic rifting event of the Arabian Tethyan margin and the Zagros passive continental margin setting of the Jurassic-Middle Cretaceous, the tectonic evolution during the Upper Cretaceous was governed by the closure of the NeoTethys and the collision of the Arabian and lranian plates. The southward obduction of Tethyan ophiolites on the Arabian margin prior to collision occurred along the Zagros belt in the Coniacian-Santonian [*Ricou*, 1976; *Berberian and King*, 1981].

[10] During the late Cretaceous, the basinal Gurpi Formation covered nearly the entire Zagros basin in response to the flexure of the Arabian plate following ophiolite emplacement. During the Paleocene-Eocene, the MFF isolated two subbasins in the foreland basin, a shallow one to the NE in which clastics and carbonates accumulated and a deeper basin to the SW where shales of the Pabdeh Formation were deposited [*Sepher and Cosgrove*, 2004]. In the Oligocene, the shallow marine limestones of the Asmari Formation deposited unconformably above the Pabdeh Formation in some places of the SW Zagros basin and also covered the Jahrom Formation in the NE Fars region. Above, the Fars Group (Gachsaran, Mishan, and Agha Jari formations) spans the period from the Miocene to Pliocene; these formations represent a first-order regressive sequence and their succession reflects the progressive infilling of the Zagros foreland basin (Figure 4).

[11] The onset of the Arabia-Eurasia collision, the initiation and the propagation of folding in the Zagros belt and the Cenozoic flexural subsidence of the Arabian margin may be constrained by the study of the synorogenic sedimentary deposits and local synfolding unconformities. According to *Hessami et al.* [2001], early fold development occurred on the margin as soon as the Paleocene probably in relation with the (still ongoing?) ophiolitic nappe emplacement, marked by the unconformable attitude of the Jahrom Formation. above the Pabdeh Formation. *Sherkati et al.* [2005, submitted manuscript, 2005] alternatively proposed that the onset of collision occurred during the Asmari period and that the onset of folding rather occurred at early Miocene times. This is in agreement with the age of inception of collision proposed by *Agard et al.* [2005]. Because of the obliquity of the convergence, continental collision probably began in the Oligocene at the northern promontory of the Arabian plate [*Yilmaz et al.*, 1993] and in the Miocene to the SE [*Stoneley*, 1981], meanwhile the final closure of the Bitlis-Zagros suture [*Sengör et al.*, 1985].

[12] The Zagros SFB began to develop as soon as Oligocene–early Miocene times toward the Arabian craton. The main phase of folding is thought to have occurred since the (middle) upper Miocene and during the Pliocene [*Berberian and King*, 1981; *Hessami et al.*, 2001; *Sherkati and Letouzey*, 2004]; intraformational unconformities and growth strata in the Upper Agha-Jari Formation suggest coeval development of most folds of the Zagros throughout

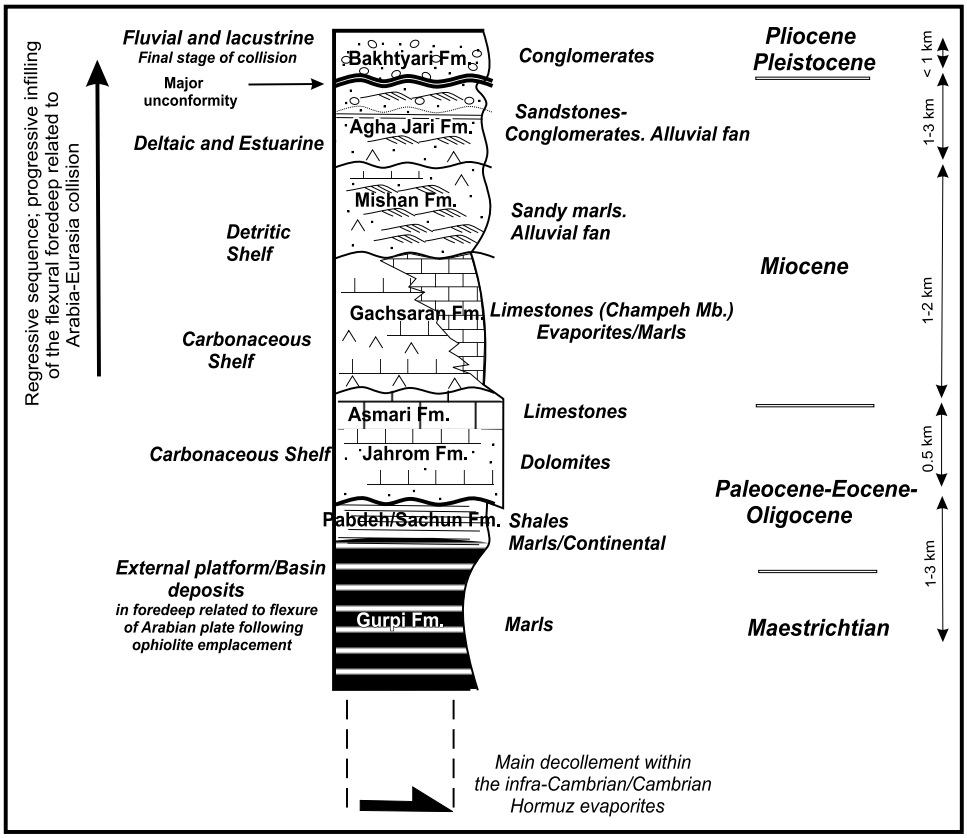

Figure 4. Main characteristics of the late Cretaceous-Cenozoic sedimentary units of the Fars.

the belt at that time. During the late Pliocene-Pleistocene, the whole Zagros belt underwent general uplift, while the coarse conglomerates of the Bakhtyari Formation deposited unconformably above the folded Agha-Jari Formation. The local tilted attitude of these conglomerates indicates recent, if not current, folding.

3. Structural Style of the Fars Area

[13] The SFB is characterized by a first-order remarkable train of folds (Figures 5 and 6). These folds consist of widely spaced open anticlines with wavelength typically of 15–20 km and length of 100km and more. Most are underlined by the limestones of the Asmari-Jahrom formations. The rather symmetric attitude of most fold limbs supports the absence of major thrusts within the folded cover. The overall constant wavelength of the folds is consistent with a single master decollement lying within the Late Proterozoic–Early Cambrian Hormuz salt [*Colman-Sadd*, 1978]. The absence of multiwavelength anticlines strongly suggests the absence of any other important decollement level in the cover; the Triassic evaporites (Dashtak Formation), one of the major intermediate decollement level recognized in the western coastal and subcoastal Fars [e.g., *Sherkati*, 2004], presumably no longer behaves as a decollement horizon in the area of interest since the facies changes to dolomites toward NE. The style of folding is therefore mainly that of large-scale detachment folding above the Hormuz evaporites, although some forced folds (i.e., folds forced by slip along underlying basement faults) are likely [e.g., *Sattarzadeh et al.*, 2000]. Between the HZF and the Surmeh-Ghir Thrust, the large anticlines alternate with tight synclines filled by synorogenic deposits (mostly the Agha-Jari Formation).

[14] A striking morphological characteristic of the Zagros belt in the Fars area is the topographic step across the MFF. This step, about 500–1000 m high, outlines the rise of Cretaceous rocks up to the surface within the cores of the anticlines. A second topographic step vanishing eastward and corresponding to the 1500 m elevation contour can locally be observed across the Surmeh-Ghir thrust where it connects to the Karebass Fault (Figures 3b and 6). Together with information derived from seismicity, these topographic observations can be used to infer that, in the Fars, the Precambrian basement is involved in collisional shortening [*Berberian*, 1995; *Sherkati and Letouzey*, 2004]. Most earthquakes are thought to occur on "blind active thrust faults" that do not reach the surface [*Berberian*, 1995]. *Jackson* [1980] proposed that NE dipping normal faults formed in response to the rifting of Iran from Arabia during the Mesozoic and located beneath the sedimentary cover, are now reactivated as high-angle reverse faults. Strike-slip-type earthquakes are

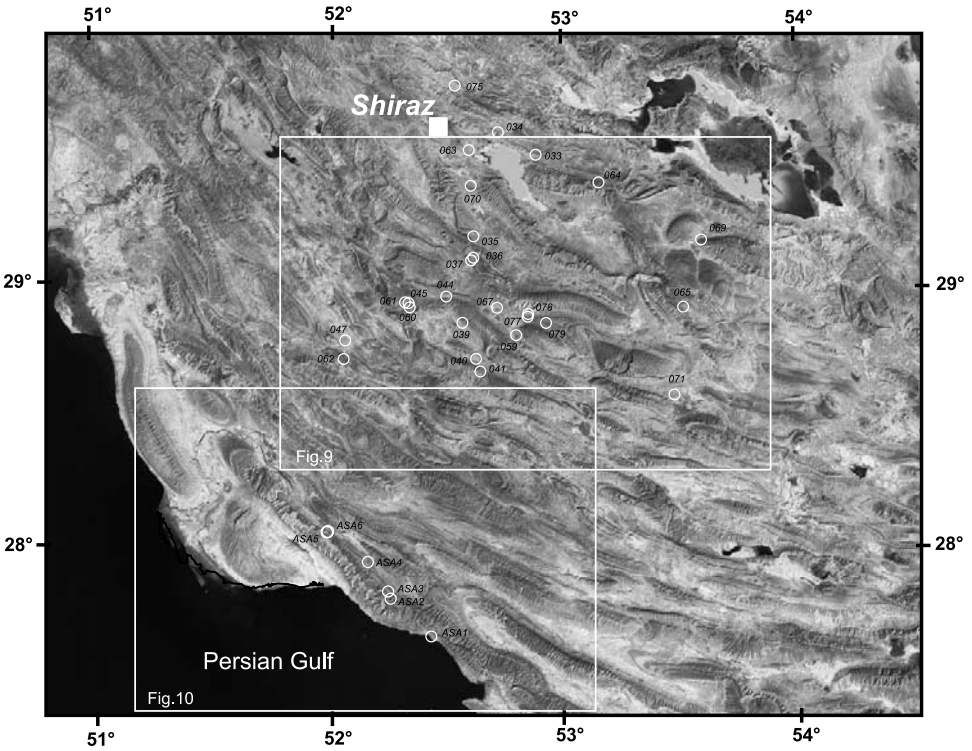

Figure 5. Landsat TM image of the area investigated and location of sites where microtectonic analyses have been carried out.

clearly related to the Kazerun-Borazjan/Karebass/Sabz-Pushan fault zones which likely correspond to basement wrench faults.

[15] The schematic section of Figure 6 aims at illustrating the structural style of the area investigated. This section has been built using surface observations of structural style and bedding dips as well as available well data and 1/100 000 National Iranian Oil Company (NIOC) geological maps. Focal mechanisms of earthquakes [*Tatar et al.*, 2004; *Talebian and Jackson*, 2004] have been additionally projected on the section in order to highlight basement tectonics (Tables 1 and 2 and section 4.1). The section shows that the structural elevation in the Fars area remains constant over 200–300 km north of the MFF, indicating that shortening is nearly homogeneously distributed across the width of the belt. The structural style of the Fars is therefore very different from the Dezful area where the structural elevation gradually increases from the foreland to the hinterland

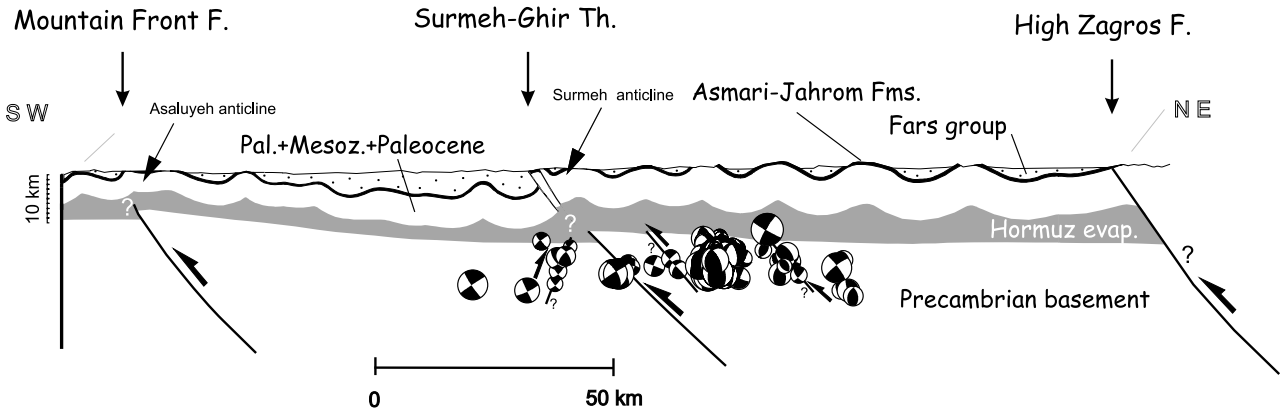

Figure 6. Schematic geological cross section across the area investigated (location on Figure 3b) (modified and simplified after *DeBoisgrollier* [2004]). Earthquake focal mechanisms from *Talebian and Jackson* [2004] and *Tatar et al.* [2004] have been projected on the section in order to highlight basement tectonics. The sizes of the focal mechanisms are proportional to the magnitude of earthquakes.

Table 1. Results of Stress Tensor Determination Based on Focal Mechanisms of Moderate Earthquakes[a]

Date	Hour	Latitude	Longitude	M_w	Az1	P1	R1	Az2	P2	R2	*Dp*
Earthquakes Whose Focal Mechanisms Constrained by P and SH Body Wave Modeling											
23 Jun 1968	09.16	029.75	051.26	5.5	136	45	088	319	45	092	
10 Apr 1972	02.06	028.41	052.79	6.7	322	40	098	132	50	083	10.0
22 Apr 1976	17.03	028.69	052.12	5.7	312	52	080	148	39	103	07.0
2 Feb 1985	20.52	028.36	052.97	5.6	128	37	091	307	53	089	11.0
7 Aug 1985	15.43	027.86	053.04	5.4	290	56	088	114	34	093	17.0
12 Jul 1986	07.54	029.91	051.56	5.5	004	73	−159	268	70	−018	07.0
11 Aug 1988	16.00	029.95	051.57	5.5	003	69	−175	271	85	−021	07.0
11 Aug 1988	16.04	029.90	051.66	5.8	350	82	−166	258	76	−008	09.0
6 Dec 1988	13.20	029.89	051.63	5.6	357	74	−164	262	73	−017	10.0
1 Mar 1994	03.49	029.14	052.63	5.9	149	75	177	239	87	015	13.0
20 Jun 1994	09.09	029.05	052.66	5.8	255	74	−003	346	87	−164	09.0
24 May 1996	06.35	027.85	053.57	5.0	109	43	081	301	47	098	06.0
13 Nov 1998	13.01	027.76	053.62	5.4	104	63	073	318	32	120	07.0
6 May 1999	23.00	029.50	051.88	6.1	049	77	−012	142	78	−167	07.0
Harvard CMT Solutions											
16 Apr 1981	10.16	029.82	051.48	5.2	351	34	144	111	71	061	15.0
18 Feb 1983	07.40	027.91	053.82	5.2	272	20	094	088	70	089	06.0
2 May 1986	03.18	028.00	053.31	5.5	107	47	057	331	52	121	15.0
3 May 1986	10.37	027.98	053.33	5.2	111	33	060	325	62	108	15.0
20 Dec 1986	23.47	029.90	051.58	5.4	348	70	−179	257	89	−020	15.0
30 Aug 1988	17.30	029.96	051.72	5.1	242	57	−009	337	83	−147	16.0
3 May 1989	09.13	030.00	051.67	5.2	153	55	−166	055	78	−036	15.0
16 Dec 1990	22.18	029.00	051.31	5.7	332	23	097	144	67	087	15.0
6 Jan 1993	22.51	029.04	052.13	5.4	248	76	000	339	90	−166	15.0
29 Mar 1993	15.20	028.01	052.74	5.2	104	28	072	305	64	099	13.0
29 Mar 1994	07.56	029.20	051.36	5.1	334	40	104	136	52	079	07.0
30 Mar 1994	19.55	028.98	052.79	5.4	148	71	177	239	87	019	33.0
3 Apr 1994	06.51	028.93	052.76	5.2	047	69	−011	142	79	−159	33.0
18 Nov 1996	11.52	029.94	51.56	5.2	177	62	−177	085	87	−028	33.0
5 May 1997	15.11	027.07	053.89	5.0	296	52	128	064	52	052	15.0
30 Apr 1999	04.20	027.84	053.54	5.1	321	53	134	082	55	047	45.0
24 Sep 1999	19.17	028.65	051.33	5.2	148	29	121	294	65	074	33.0
31 Oct 1999	15.09	029.41	051.81	5.2	117	34	067	324	58	105	33.0
1 Mar 2000	20.06	028.40	052.85	5.0	049	26	055	267	69	106	15.0
13 Sep 2000	13.09	027.82	051.68	4.9	126	26	144	249	75	068	44.0
First Motion Fault Plane Solutions											
14 Sep 1968	13.48	028.34	053.18	5.8	108	60	090	288	30	090	07.0

[a]See *Talebian and Jackson* [2004]. For each earthquake, date, hour, latitude/longitude of epicenter, magnitude (M_w), azimuth/dip/rake of nodal planes 1 and 2 in degrees (Az/P/R), and depth of focus in km (*Dp*) are given. For the stress tensor solution the lowest acceptable value of the ratio ω (ω_{ACC} = 45%, see text), trend/plunge of σ_1, σ_2, and σ_3 in degrees (T/Pl, Tσ_1 = 209, Plσ_1 = 01, Tσ_2 = 119, Plσ_2 = 02, Tσ_3 = 322, Plσ_3 = 88); value of the Φ ratio (Φ = 0.08); number of mechanisms consistent with the tensor (N = 34); number of rejected mechanisms (Nr = 1); and mean value of the ratio ω (mean ω = 76), and mean value of the angular deviation α of the shear stress with respect to actual slip (mean α = 24) are given.

where deeper rocks are progressively exposed [*McQuarrie*, 2004; *Sherkati and Letouzey*, 2004]. In addition, the noticeable absence of large overthrusts in the Fars cover indicates that shortening likely remained limited in amount. The long period of activity along the MFF and the Surmeh-Ghir thrust (marked for the latter by the localized subsidence in the footwall of the thrust during deposition of the Mishan formation [*Motiei*, 1993; *Mouthereau et al.*, 2005] as well as the location of the oldest stratigraphic exposures in the cores of the anticlines located above these basement faults suggest that the cover, although largely decoupled from the basement, presumably did not slide above it of a large amount. In the westernmost Fars, Sherkati et al.(submitted manuscript, 2005) estimated, based on section balancing, an amount of cover shortening of 34 km in the SFB and a total shortening of 50 km throughout the entire belt. In the southeastern Fars, *Molinaro et al.* [2005] estimated an amount of cover shortening of 15–20 km in the SFB and a total shortening of 45 km throughout the entire belt. In contrast with these estimates considering basement-involved shortening, *McQuarrie* [2004] proposed an amount of shortening of 67 km based on pure thin-skinned tectonic style.

4. Methods Used for Determining Late Cenozoic and Modern Stress Regimes

[16] We have first performed the inversion of earthquake focal mechanisms in order to characterize the present-day stress pattern in the western Fars. In order to go back in the past and to bring constraints on the regional late Cenozoic tectonic evolution and on the kinematics of folding, we further reconstructed the Cenozoic paleostress patterns based on small-scale brittle deformation, such as striated microfault surfaces and veins. This microtectonic study was combined with the analysis of the macrotectonic features

Table 2. Results of Stress Tensor Determination Based on Focal Mechanisms of Small Earthquakes[a]

Date	Hour	Latitude	Longitude	M_w	Az1	P1	R1	Az2	P2	R2	*Dp*
14 Nov 1997	13.47	027.90	053.16	3.0	295	65	081	135	26	108	18.0
16 Nov 1997	00.07	028.33	053.28	3.0	129	80	085	335	11	115	12.8
16 Nov 1997	7.27	028.58	052.99	2.1	115	65	070	335	31	125	15.8
16 Nov 1997	18.04	028.37	053.10	2.0	165	65	−168	070	79	−025	10.7
17 Nov 1997	00.50	028.06	052.96	2.2	300	20	099	110	70	086	12.8
17 Nov 1997	01.39	028.05	052.96	1.8	300	20	099	110	70	086	12.3
17 Nov 1997	02.36	028.04	052.98	1.9	140	45	116	285	50	066	16.8
17 Nov 1997	02.39	028.05	052.97	2.1	150	50	132	275	55	051	14.5
17 Nov 1997	02.58	028.05	052.97	2.6	155	60	143	265	59	035	12.2
19 Nov 1997	22.57	028.28	053.57	2.1	350	80	−153	255	63	−011	18.0
19 Nov 1997	23.02	028.29	053.57	2.3	350	80	−153	255	63	−011	12.5
20 Nov 1997	23.47	028.34	052.96	1.9	315	30	121	100	64	073	14.6
21 Nov 1997	14.51	027.93	053.15	2.1	105	40	090	285	50	090	09.1
22 Nov 1997	20.21	028.22	052.97	2.0	330	65	147	075	61	028	15.1
26 Nov 1997	23.52	028.41	053.09	1.6	320	35	110	115	57	076	13.8
27 Nov 1997	01.21	028.41	053.08	1.7	320	35	110	115	57	076	13.9
28 Nov 1997	08.15	028.08	053.27	2.5	110	70	086	300	20	099	13.6
30 Nov 1997	02.01	028.04	053.05	1.7	110	50	103	270	41	074	10.1
30 Nov 1997	02.57	028.25	053.26	2.7	120	65	101	275	27	067	15.8
1 Dec 1997	12.26	028.03	053.05	2.4	085	50	041	325	59	131	11.8
2 Dec 1997	06.28	028.22	052.97	2.4	310	75	−161	215	72	−015	13.7
3 Dec 1997	16.16	028.29	053.32	2.0	250	65	−011	345	79	−154	12.7
4 Dec 1997	03.16	028.28	053.36	2.8	335	75	161	070	72	015	15.0
10 Dec 1997	23.07	028.17	053.16	2.2	285	45	086	110	45	093	12.3
11 Dec 1997	17.01	028.14	053.05	2.2	145	75	075	010	20	133	13.2
11 Dec 1997	17.19	028.15	053.05	2.0	145	75	075	010	20	133	13.8
14 Dec 1997	20.46	028.46	053.20	3.6	100	40	068	307	53	107	13.9
15 Dec 1997	04.38	028.29	053.62	2.4	070	65	011	335	79	154	19.0
18 Dec 1997	00.26	028.34	053.25	2.2	070	60	054	305	45	135	14.0
21 Dec 1997	08.57	028.38	053.18	2.8	330	60	−137	215	53	−038	11.4
21 Dec 1997	18.48	028.35	053.27	2.0	265	55	055	135	47	128	15.2
22 Dec 1997	19.24	028.11	053.48	1.8	340	75	161	075	72	015	08.3
22 Dec 1997	20.45	028.12	053.46	1.9	340	80	153	075	63	011	09.5
22 Dec 1997	21.33	028.12	053.45	1.7	340	80	153	075	63	011	08.6
23 Dec 1997	01.34	028.12	053.46	3.3	350	80	−153	255	63	−011	15.2
25 Dec 1997	07.10	028.35	053.06	2.0	240	50	036	125	63	134	12.2
25 Dec 1997	11.16	028.13	053.48	2.2	350	80	−153	255	63	−011	10.2
26 Dec 1997	05.40	028.09	053.47	2.8	345	80	−153	250	63	−011	14.1
26 Dec 1997	07.08	028.10	053.47	2.7	340	80	−153	245	63	−011	12.7
26 Dec 1997	08.07	028.08	053.48	3.3	090	75	018	355	72	164	15.6
26 Dec 1997	11.34	028.11	053.46	3.3	090	75	018	355	72	164	14.1
26 Dec 1997	12.38	028.08	053.46	3.1	090	75	018	355	72	164	12.0
27 Dec 1997	02.00	028.09	053.47	3.1	345	80	−153	250	63	−011	15.3
27 Dec 1997	15.21	028.06	053.49	3.3	340	80	153	075	63	011	13.5
27 Dec 1997	19.31	028.31	053.30	1.8	250	55	−017	350	76	−143	13.6
28 Dec 1997	01.30	028.12	053.46	3.3	335	80	−153	240	63	−011	12.4
28 Dec 1997	07.11	028.11	053.46	3.2	320	80	153	055	63	011	11.1
28 Dec 1997	17.05	028.01	053.46	2.7	335	75	161	070	72	015	11.1
29 Dec 1997	00.00	028.10	053.48	3.7	335	75	161	070	72	015	14.7
29 Dec 1997	03.06	028.10	053.47	3.3	320	65	168	055	79	025	12.6

[a]See *Tatar et al.* [2004]. For each earthquake, date, hour, latitude/longitude of epicenter, magnitude (M_w), azimuth/dip/rake of nodal planes 1 and 2 in degrees (Az/P/R), and depth of focus in km (*Dp*) are given. For the stress tensor solution the lowest acceptable value of the ratio ω (ω_{ACC} = 65%, see text), trend/plunge of σ_1, σ_2, and σ_3 in degrees (T/Pl, Tσ_1 = 206, Plσ_1 = 08, Tσ_2 = 096, Plσ_2 = 69, Tσ_3 = 299, Plσ_3 = 20); value of the Φ ratio (Φ = 0.13); number of mechanisms consistent with the tensor (N = 44); number of rejected mechanisms (Nr = 6); and mean value of the ratio ω (mean ω = 83), and mean value of the angular deviation α of the shear stress with respect to actual slip (mean α = 17) are given.

based on fieldwork and morphostructural studies using Landsat TM images.

4.1. Determining Contemporary Stress Regimes From Inversion of Earthquake Focal Mechanisms

[17] Intense seismicity is distributed throughout the 200–300 km width of the Zagros mountain belt [*Berberian*, 1995; *Talebian and Jackson*, 2004] (Figure 1b). In contrast to the other seismic regions of Iran (e.g., Alborz, Kopet-Dag), this seismicity is of low magnitude (only small to moderate earthquakes). *Jackson and McKenzie* [1988] proposed that the Zagros suffers predominantly aseismic deformation. This is confirmed by the comparison of seismic and geodetic strain rates which indicates mainly aseismic deformation in the Zagros [*Masson et al.*, 2005]. A possible

reason of this particular behavior of the Zagros could be the large thickness (more than 8–10 km) of the sedimentary coverage of the Zagros, decoupled from the basement by the Hormuz salt layer at its base: The vertical thickness of the seismogenic layer, between 10 and 14 km according to microseismicity studies [*Tatar et al.*, 2004], would be too thin to generate large earthquakes which cannot propagate upward due to the salt layer.

[18] Various sets of earthquake focal mechanisms are however available for the Zagros. The first data set used for characterizing the present-day state of stress consists of the focal mechanisms of moderate earthquakes (magnitude M_w between 4.9 and 6.7) reported by *Talebian and Jackson* [2004] for the period 1968–2000. These focal mechanisms include mechanisms constrained by *P* and *SH* body wave modeling, Harvard centroid moment tensor (CMT) solutions and first motion fault plane solutions (Table 1). The second set of data used hereinafter consists of focal mechanisms of relocated microearthquakes reported by *Tatar et al.* [2004] for the period November–December 1997 and spread over the investigated area (Table 2). Magnitudes (Ml) range between 1.7 and 4.1. Because microearthquakes are likely related to the internal deformation of the crust (*P* or *T* axes) rather than to major displacements (slip vectors) as larger earthquakes are [*Tatar et al.*, 2004], both types of data were used separately to carry out inversion.

[19] In the Zagros, the absence of a dense local seismological network results in a poor coverage of seismological stations. Because of this poor coverage and the absence of a precise velocity model for crustal structure, earthquake locations are generally insufficiently accurate to definitely answer questions concerning the relationship between seismicity and precise location of active faults or precise focal depths. Most of the reliable focal mechanisms of moderate earthquakes in the Zagros have been determined using first motion polarities recorded by the long-period stations of Worldwide Standard Seismological Network [*McKenzie*, 1972, 1978] or using body wave modeling [*Jackson and McKenzie*, 1984; *Baker et al.*,. 1993; *Maggi et al.*, 2000]. For the moderate earthquakes used in this study [*Talebian and Jackson*, 2004], estimates of foci depths range from 6 to 44 km (Table 1). For the small-size earthquakes, *Tatar et al.* [2004] found that they occur within the 8–19 km range of depth, mainly between 10 and 14 km, with a peak of frequency at 11 km. The 8–19 km depth range possibly includes the cover/basement transition, which remains poorly constrained because of the absence of published seismic and borehole data. Considering 8–9 km as a minimum estimate of depth to basement, a depth roughly confirmed by the results of aeromagnetic surveys [*Morris*, 1977] and adopted in recent attempts at balancing cross sections [*Sherkati*, 2004; *Molinaro et al.*, 2005], most of the earthquakes used in the present work are located in the basement: For the moderate-size earthquakes, only nine are reported by *Talebian and Jackson* [2004] in the area of interest as having occurred at depth shallower than 8 km; for the small-size earthquakes, none occurred at depth shallower than 8 km (Table 2). Because of uncertainties on both earthquake location and accurate thickness of the sedimentary cover, an a priori separation of focal mechanisms of earthquakes occurring in the cover and in the basement has not been done. In addition, the number of earthquakes possibly reflecting cover seismicity (9 events) would have been too limited to allow a reliable stress inversion. Consequently, despite the occurrence of the Hormuz decollement at the base of the cover which likely acts as a seismic boundary for much of earthquakes [*Masson et al.*, 2005], the few (possible) cover earthquakes have been kept together with basement earthquakes to carry out inversion. Stress inversion results show that these few mechanisms fit well with the stress solution computed with the total set of focal mechanisms of moderate earthquakes (see section 5.1).

[20] To characterize the present-day state of stress of the western Fars, we applied stress inversion method to the focal mechanism database. Stress inversion methods generally assume a uniform state of stress within the study area. In contrast to the inversion of fault slip data, standard inversion of earthquake data does not a priori discriminate between the active and the virtual nodal planes. The aim of the inversion of focal plane data is the determination of a regional stress tensor that satisfies most, if not all, reconstructed double couple focal mechanisms of individual earthquakes in the area of interest. In contrast to the simple interpolation of isolated *P*-*T* axes directions, the method takes the entire information from the focal mechanisms in terms of principal stress axes and ratio between differential stress magnitudes.

[21] In this paper, we used the new inverse method proposed by *Angelier* [2002]. This new inversion process is based on the slip shear stress component (SSSC) criterion, which is the component of stress acting in the slip direction of a fault. The ratio between the SSSC and the maximum shear stress $(\sigma_1 - \sigma_3)/2$, called ω, reflects the quality of the individual fit obtained through the inversion; this ratio varies from -100% (total misfit) to 100% (perfect fit). The inversion process maximizes ω, which is equivalent to minimizing the angular deviation α of the shear stress with respect to actual slip and at the same time to maximizing the shear stress for all the data taken together. The mean value of the ω ratio (mean ω) provides an estimator of the quality of the computed average stress tensor.

[22] The stress tensor solution is given in terms of 4 unknowns, which are the orientation (trend and plunge) of the three principal stress axes σ_1, σ_2, and σ_3 (with $\sigma_1 \geq \sigma_2 \geq \sigma_3$, compression considered positive) and the Φ ratio between differential stress magnitudes ($\Phi = (\sigma_2 - \sigma_3)/(\sigma_1 - \sigma_3)$, with $0 \leq \Phi \leq 1$). This ratio characterizes the shape of the stress ellipsoid, and therefore the actual nature of the stress regime (e.g., reverse/strike-slip if σ_3 is vertical and Φ close to 0).

[23] A double couple focal mechanism of earthquakes involves two possible, mutually exclusive, fault slips. For each nodal plane the potential slip vector is perpendicular to the other plane. If the focal mechanism and the stress tensor are perfectly consistent, the SSSC value is unique regardless

of the nodal plane acting as the fault. The SSSC criterion is thus ideal to avoid the intrinsic ambiguity of focal mechanisms. The striking originality of the method is that since it is based on the Tresca criterion rather that on an explicit Mohr-Coulomb criterion, it requires no choice between the nodal planes prior to or during the inversion.

[24] To determine whether a stress inversion is significant or not, a refining process involves successive inversions with a progressively increasing requirement for good individual fits (i.e., an increasing minimum acceptable value, ω_{ACC}, of ω). This process allows determination of the level of data rejection consistent with the data accuracy (see *Angelier* [2002] for details). Note that to evaluate the validity of the results, the number of rejected data and the largest acceptable misfit are more important than the average misfits and their standard deviations, which can be made artificially small by choosing a severe fit requirement resulting in many rejected data.

4.2. Determining Paleostress Regimes From Inversion of Fault Slip Data

4.2.1. Assumptions and Basic Mechanical Principles

[25] The kinematics of a fault population is defined using striations observed on mesoscale fault planes at many sites (Figure 7). For each fault, strike, dip, slickenside rake and polarity of movement are measured and determined in the field. The main objective is to define the successive Cenozoic states of stress and the related faulting events and their probable significance in relation to regional tectonic events. Other stress indicators, such as veins and stylolites, although not used in the inversion process, help to constrain extensional and compressional trends, respectively. The methodology of fault kinematic studies to determine paleostress fields and identify temporal and spatial changes in stress states has been used in many areas worldwide over the past 30 years [e.g., *Letouzey*, 1986; *Bergerat*, 1987; *Lacombe et al.*, 1990; *Bellier and Zoback*, 1995; *Ozden et al.*, 2002]. To determine the stress fields responsible for Cenozoic deformation in the investigated area, we have carried out a quantitative inversion of distinct families of slip data determined at each individual site, using the method proposed by *Angelier* [1990].

[26] Fault slip inversion method assumes that (1) the analyzed body of rock is physically homogeneous and isotropic and if prefractured, is also mechanically isotropic, i.e., the orientation of fault planes is random, (2) the rock behaves as a rheologically linear material [*Twiss and Unruh*, 1998], and (3) displacements on the fault planes are small with respect to their lengths and there is no ductile deformation of the material and thus no rotation of fault planes. Moreover, the computation assumes that (4) a tectonic event is characterized by a single homogeneous stress tensor, (5) the slip responsible for the striation occurs on each fault plane in the direction and the sense of the maximum resolved shear stress on each fault plane (Wallace-Bott principle), the fault plane being the preexisting fracture, and (6) the slip on each of the fault planes is independent of each other. Because in the cover of the SFB of the Fars region the train of folds is regular and almost devoid of major thrust zones at least reaching the surface (Figure 6), paleostress reconstructions reported herein therefore meet the assumptions of stress homogeneity and low finite internal strain and likely yield the regional paleostresses of interest.

[27] The basic principle consists of finding the best fit between the observed directions and senses of slip on numerous faults and the theoretical shear stress induced on these planes by the tensor solution of the inverse problem. As for inversion of earthquake focal mechanisms, the results are the local orientation (trend and plunge) of the three principal stress axes σ_1, σ_2, and σ_3 and the Φ ratio. The quality of the tensor calculated is given by numerical estimators such as the average angle between the computed shear stresses and the actual striations on fault surfaces (Table 3). Uncertainties in the principal stress directions depend mainly on the geometric distribution of fault slip data; under optimal conditions, the accuracy on the trend and plunge of stress axes is better than 10°.

4.2.2. Establishing a Relative Chronology Between Successive Faulting Events/Stress Regimes

[28] The identification and separation of successive generations of faults and related stress regimes is based on both mechanical incompatibility between fault slips (individual misfits of fault slips with the computed stress tensors) and relative chronology observations (superimposed striations on fault surfaces, crosscutting relationships between faults). In order to establish a time distribution of tectonic regimes, dating of the brittle structures also requires stratigraphic information about the age of the deformed units and/or evidence of syndepositional tectonism. Particular attention was also paid to horizontal axis rotations of rock masses due to folding [e.g., *Yamaji et al.*, 2005]. Where tilted bedding is observed as a result of folding, several cases deserve consideration, because faults may have formed before, during or after folding. For instance, prefolding strike-slip faults, a common feature in the SFB, can be unambiguously identified by the attitude of the striations which always lie within the bedding whatever strata attitude, and thus have to be interpreted in their back-rotated attitude (Figures 8a and 8b). Following *Anderson* [1951], we assume that away from major fault zones, one of the three principal stress axes of a tensor is generally vertical. If a fault set formed before folding and was secondarily tilted with the bedding, the tensor calculated on this set does not display a vertical axis. Instead, one of the stress axes is generally found perpendicular to bedding, whereas the two others lie within the bedding plane (Figure 8). In such a case, the fault system is interpreted after back tilting to its initial position. Within a heterogeneous fault population this geometrical reasoning allows separation of data subsets based on their age relative to fold development. In the case of the very simple geometry and cylindrical character of folds in the Zagros SFB, this criterion is of primary importance for establishing a relative chronology. This criterion can be further combined with dating of fold development using unconformities and growth strata within synorogenic deposits. The chronology inferred this way is usually confirmed by identifi-

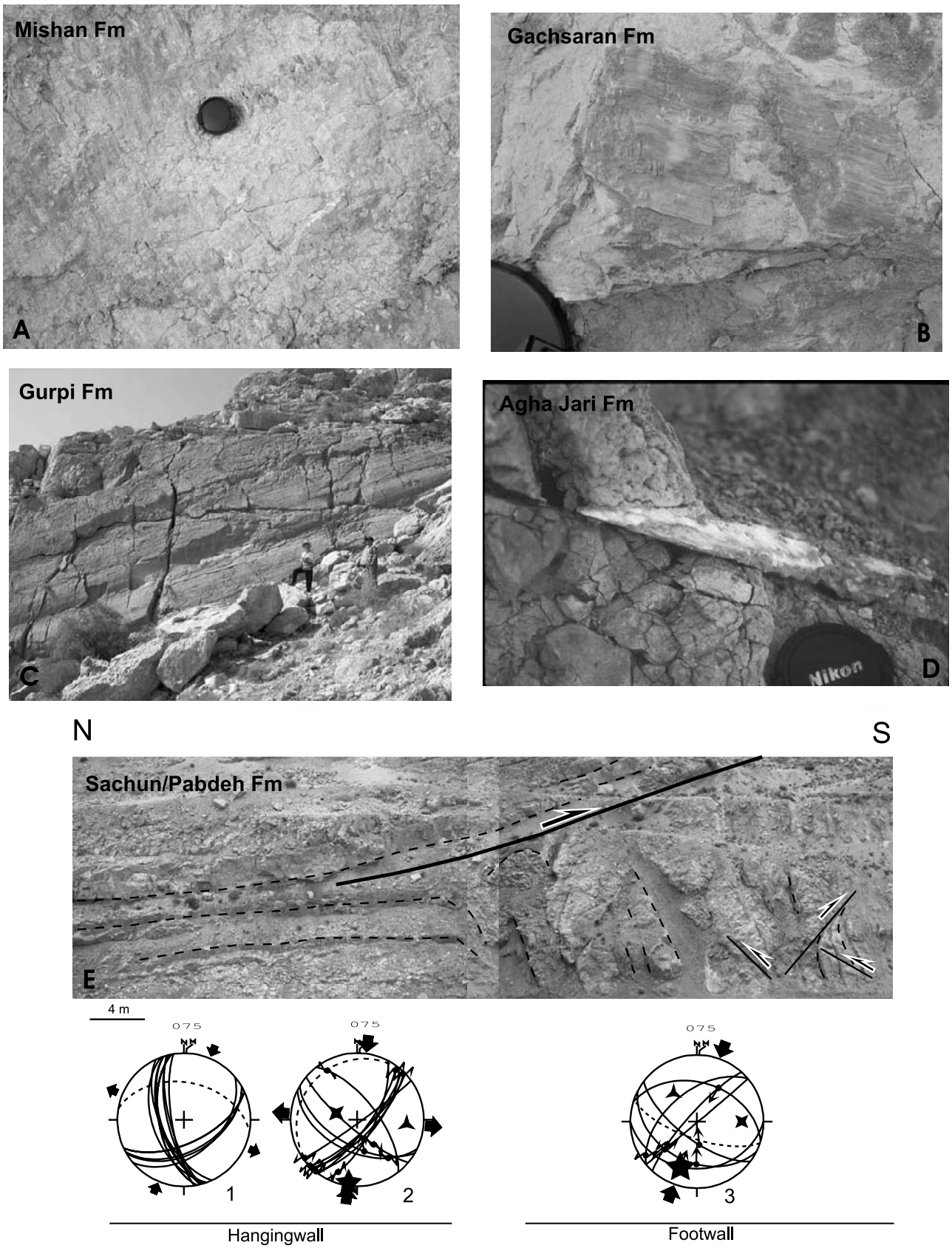
Mishan Fm
A
Gachsaran Fm
B
Gurpi Fm
C
Agha Jari Fm
Nikon
D
N
S
Sachun/Pabdeh Fm
E
4 m
075
075
075
1
2
3
Hangingwall
Footwall

Figure 7

Table 3. Results of Stress Tensor Determination Based on Fault Slip Data[a]

Site	Location	Formation	Trend (Plunge) of the Principal Stress Axes			Ratio Between Differential Stresses Φ	Number of Data	α, deg
			σ_1	σ_2	σ_3			
33	29°27.55/52°55.2	Jahrom	5		95		21F′	
34	29°32.72/52°45.6	Asm- Jahr	035 (00)	125 (01)	289 (89)	0.29	11F	11.7
			318 (01)	048 (06)	219 (84)	0.27	5F	9.7
35	29°09.33/52°39.28	Asmari	205 (02)[b]	069 (88)[b]	295 (02)[b]	0.12	13F	6.7
			110 (34)	329 (49)	214 (20)	0.13	8F	4.1
36	29°04.61/52°39.31	Asm-Jahr	40		130		8F′	
37	29°03.94/52°38.77	Asmari	309 (01)	343 (06)	251 (12)	0.12	13F	6.7
			132 (19)	015 (53)	234 (31)	0.12	11F	6.8
39	8°49.75/52°36.66	Asm-Jahr	36		126		25F′	
40	8°41.74/52°39.99	Gachsaran	193 (09)	102 (04)	348 (80) -	0.7	24F	6.8
41	28°38.85/52°41.05	Gachsaran	24		114		16F′	
44	28°55.77/52°32.27	Gachsaran	193 (14)	286 (10)	048 (73)	0.45	19F	8.5
			060 (06)	289 (82)	150 (06)	0	5F	8.4
			300 (24)	047 (33)	182 (47)	0.5	6F	19.5
45	28°54.24/52°22.44	Pabd-Gurpi	217 (24)	042 (66)	307 (02)	0.26	9F	6.6
47	28°45.84/52°06.49	Gachsaran	071 (10)[b]	293 (75)[b]	164 (05)[b]	0.3	29F	13
			030 (06)	156 (80)	300 (08)	0.47	9F	6.3
59	28°46.98/52°50.19	Gachsaran	223 (02)	321 (77)	132 (13)	0.1	17F	7.6
60	28°53.33/52°22.91	Asm-Jahr	190 (21)	324 (61)	093 (19)	0.16	16F	10.6
62	28°41.60/52°06.00	Cretaceous	178 (10)[b]	273 (28)[b]	071 (60)[b]	0.11	21F	9
63	29°28.79/52°38.04	Asmari	079 (04)	171 (24)	340 (65)	0.2	18F	14.2
67	28°53.20/52°45.40	Gachsaran	028 (12)	297 (04)	188 (77)	0.57	15F	7.4
			023 (12)	138 (64)	288 (23)	0.37	10F	7.6
			050 (08)	282 (76)	141 (11)	0	17F	4.8
69	29°08.69/53°37.61	Jahrom	015 (12)	285 (04)	193 (78)	0.57	11F	5.5
70	29°20.80/52°38.50	Jahrom	70		160		10F′	
71	28°33.05/53°32.37	Mishan	178		88		20F′	
75	29°43.27/52°34.63	Sachun	188 (05)	287 (63)	095 (26)	0.16	11F	12.6
			199 (28)	090 (33)	321 (44)	0	7F	6.8
			22		112		12F′	
77	28°51.28/52°53.28	Mishan	12		102		19F′	
78	28°51.74/52°53.34	Mishan	162 (02)	266 (81)	071 (09)	0.38	9F	8.9
79	28°49.82/52°57.93	Mishan	187 (13)	278 (06)	033 (76)	0.68	12F	9.8
ASA1	27°38.64/52°28.75	Cretaceous	167 (38)	338 (52)	074 (05)	0.23	9F	22.9
			200 (12)	295 (22)	083 (64)	0.46	9F	5.9
ASA2	27°47.17/52°17.43	Mishan	230 (00)	320 (14)	140 (76)	0.89	16F	4.4
ASA3	27°48.71/52°17.43	Mishan	048 (05)	317 (08)	169 (81)	0.56	10F	7.9
			077 (15)	226 (72)	344 (09)	0.53	7F	6.6
ASA4	27°55.56/52°12.34	Cretaceous	240 (06)	330 (03)	088 (83)	0.43	7F	14.8
			251 (03)	156 (56)	343 (34)	0.23	6F	4.2
ASA5	28°02.68/52°02.80	Pabd-Gurpi	022 (18)	115 (10)	232 (70)	0.58	7F	6
ASA6	28°02.45/52°01.07	Pabd-Gurpi	227 (04)	117 (78)	318 (11)	0.17	17F	11.2

[a]Trend and plunge of each stress axis are given in degrees. Ratio Φ is defined in text. F, number of striated fault planes consistent with the tensor; F′ number of extensional fractures/veins; α, average angle between actual slip and computed shear stress, in degrees.
[b]Backtilted stress axes.

Figure 7. Examples of mesoscale faults observed in the field. (a) Minor reverse fault underlined by calcite steps within the Mishan Formation south of the Sim anticline. (b) Minor strike-slip fault underlined by gypsum fibers within the Gachsaran Formation. (c) Decameter-scale strike-slip fault within the Gurpi Formation within the Asaluyeh anticline. (d) Minor reverse fault underlined by sigmoidal gypsum fibers within the Agha Jari Formation. (e) Example of outcrop used in microtectonic studies. Figure 7e corresponds to site 075, north of Shiraz. Note the consistency of the N020° compressional trend inferred from fracture analyses in both the hanging wall and the footwall of the reverse fault, suggesting the absence of significant stress/block rotation during and after folding. Diagrams illustrate fault slip data: thin curves represent fault planes and dots with double arrows (left- or right-lateral) or simple ones (centripetal-reverse/centrifugal-reverse) indicate striations. Stars indicate stress axes with five points (σ_1), four points (σ_2), and three points (σ_3). Small squares represent poles to veins. Small diamonds represent stylolitic peaks. Bedding planes are shown as dashed lines. Large arrows represent direction of compression (convergent arrows) and extension (divergent arrows).

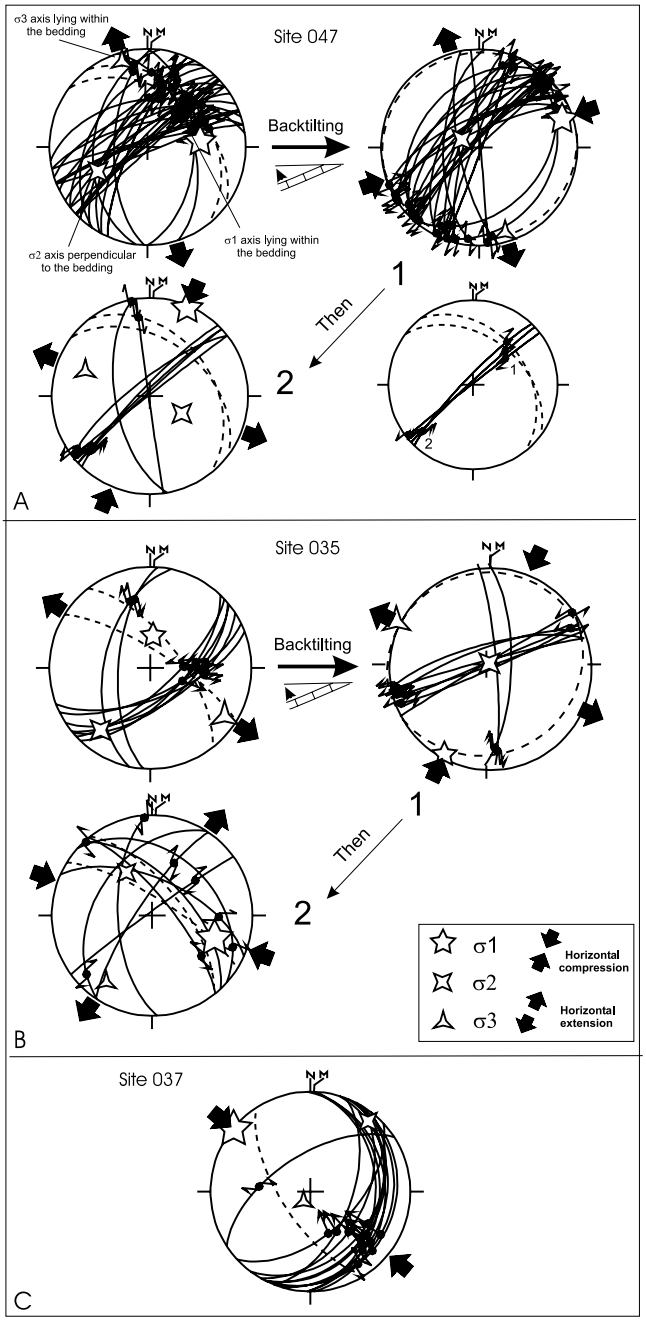

Figure 8. Example of data separation based on chronological relationships between faulting and folding. (a) Relative chronology between NE-SW and N020° compressional trends derived from faulting/folding relationships and from superimposed striations on fault surface in site 047. (b) Relative chronology between N020° and N120° compressional trends derived from faulting/folding relationships in site 035. (c) Postfolding N120° compressional trend in site 037.

cation of superimposed striations on reactivated fault surfaces where observable (Figure 8a); it therefore reliably reflects the local succession of faulting events and related stress regimes.

[29] A noticeable point arising from this study is that small-scale faulting occurs mainly before folding as layer-parallel shortening (LPS) passively tilted as folding occurs, and after fold development. The limited evidence of syn-folding faulting suggests that internal strain is mainly achieved during the early and late stages of folding, probably during two peaks of stresses which seem to predate immediately folding (buckling) and to prevail after fold tightening [*Onasch*, 1983]. During folding, shortening oblique to bedding leads to mixed simple shear deformation (bedding-parallel slip, as deduced from slickensides observed along beds) and pure shear, the latter being poorly recorded by mesoscale faulting.

[30] For the sake of clarity we only provide examples of the most significant diagrams illustrating fault slip data (Figures 9, 10, and 11). The parameters of the stress tensors are listed in Table 3.

5. Results of Tectonic Analyses

5.1. Present-Day Stress Regimes in the Western Fars

[31] Among the focal mechanisms of the moderate earthquakes reported by *Talebian and Jackson* [2004], 35 were selected as having occurred within the area of interest (latitude 27–30°; longitude 51–54°, Table 1). Most of the thrust earthquakes occur along the SW Zagros margin, between the coast of the Persian Gulf and the Surmeh-Ghir thrust zone, while strike-slip earthquakes are clearly associated with the Kazerun/Karebass/Sabz-Pushan faults (Figure 12a). The good quality of the data enabled us to require a low smallest acceptable value of individual ω (45%) (refer to *Angelier* [2002] for details). The inversion process accounts for 34 of these mechanisms, a single earthquake being rejected, and indicates a stable solution corresponding to a subhorizontal σ_1 axis trending N209° (±15) (Figure 12a) and a subvertical σ_3 axis (322 88). The value of the Φ ratio is 0.08 (within a possible range 0–0.3). This suggests that σ_2 and σ_3 axes have values close to each other and that $\sigma_2 - \sigma_3$ stress permutations are likely. This regime thus accounts for the coeval occurrence of reverse and strike-slip faulting, although the slip vectors are clearly different for thrust and strike-slip earthquakes [*Talebian and Jackson*, 2004]. This N209° direction of compression is consistent with the mean direction of the *P* axes of mechanisms of moderate earthquakes whatever the type of focal mechanisms (reverse or strike-slip) and the foci depths (events occurring in the cover (depth < ~8 km) and in the basement) (Figure 13).

[32] Focal mechanisms of microearthquakes reported by *Tatar et al.* [2004] (Table 2) indicate both reverse and strike-slip faulting in agreement with those of stronger earthquakes. However, there is no univocal relation between strike-slip mechanisms and the recognized major strike-slip faults nor between the reverse mechanisms and the Surmeh-Ghir thrust. This suggests that shortening is distributed and accommodated by both reverse faults and right-lateral strike-slip faults presumably interconnected at the local scale. Among the 73 earthquake focal mechanisms reported by *Tatar et al.* [2004] only 50 were retained for the stress

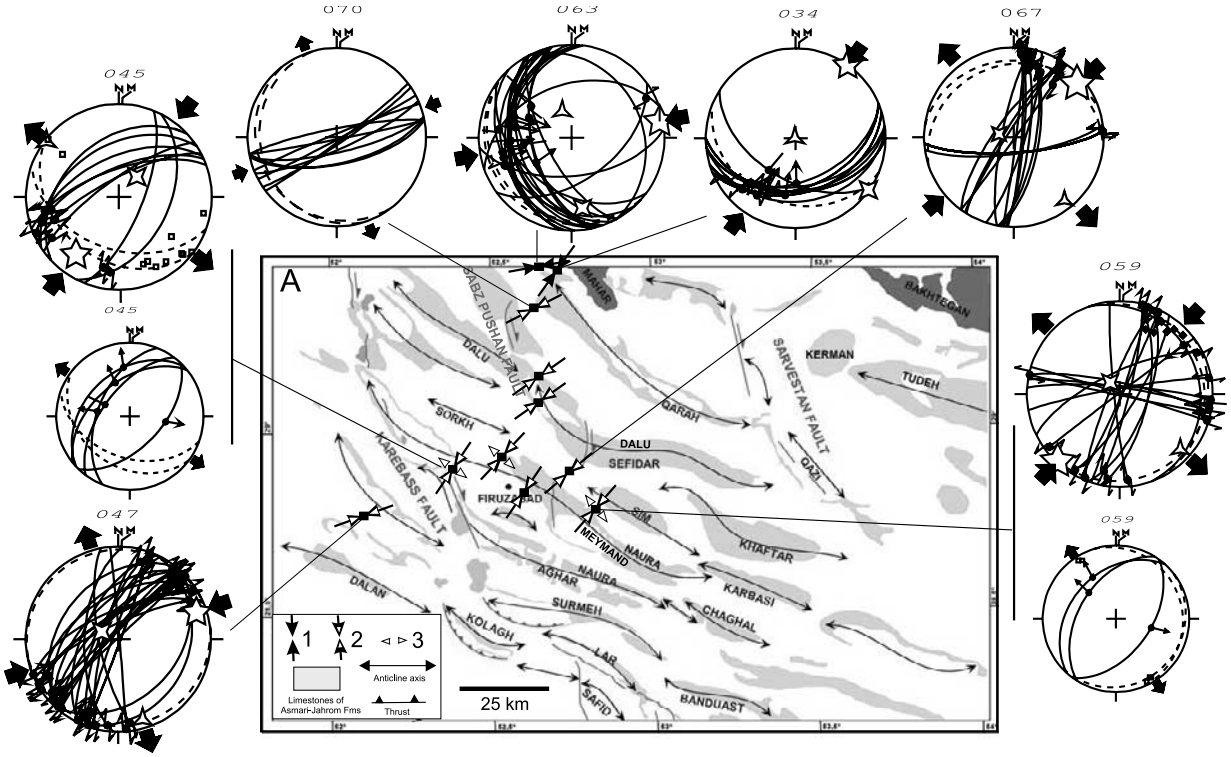

NE-SW compression

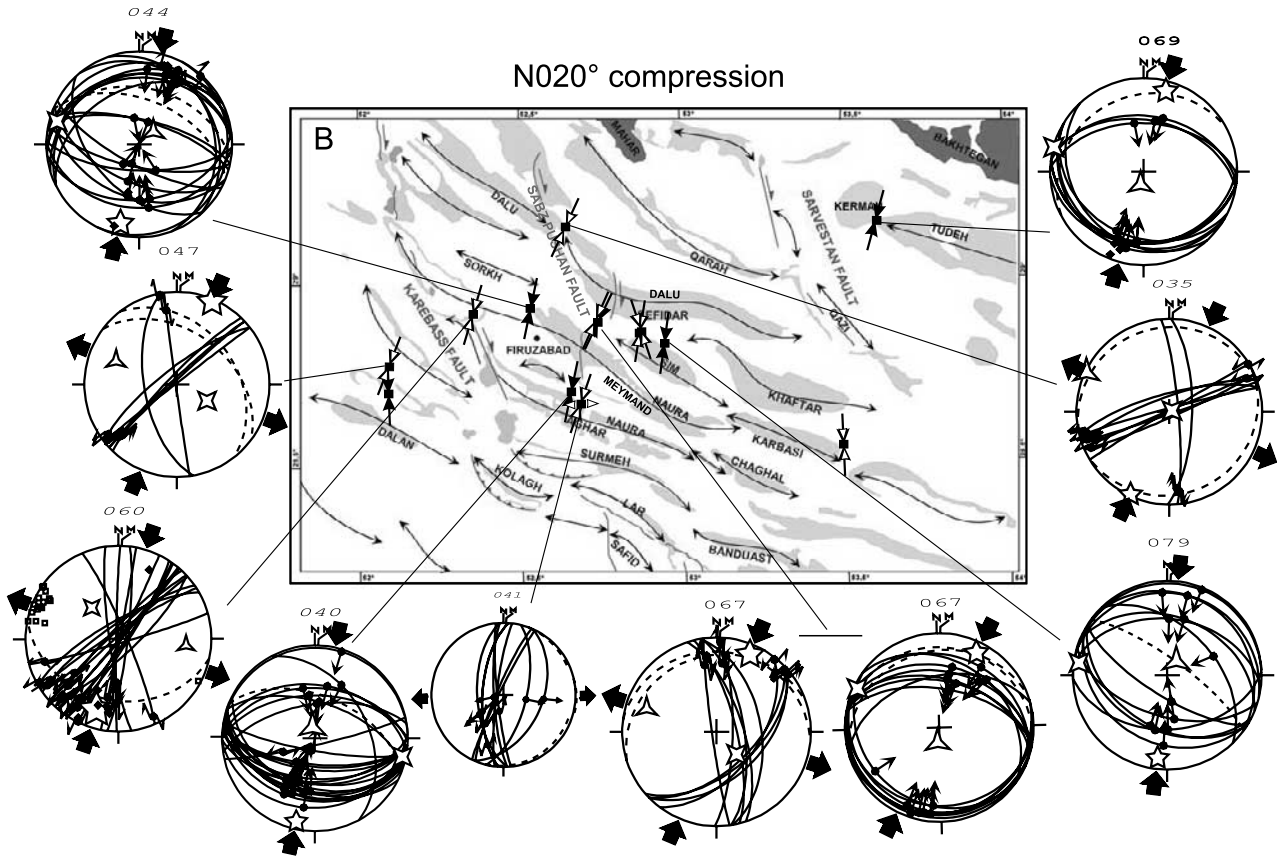

N020° compression

Figure 9

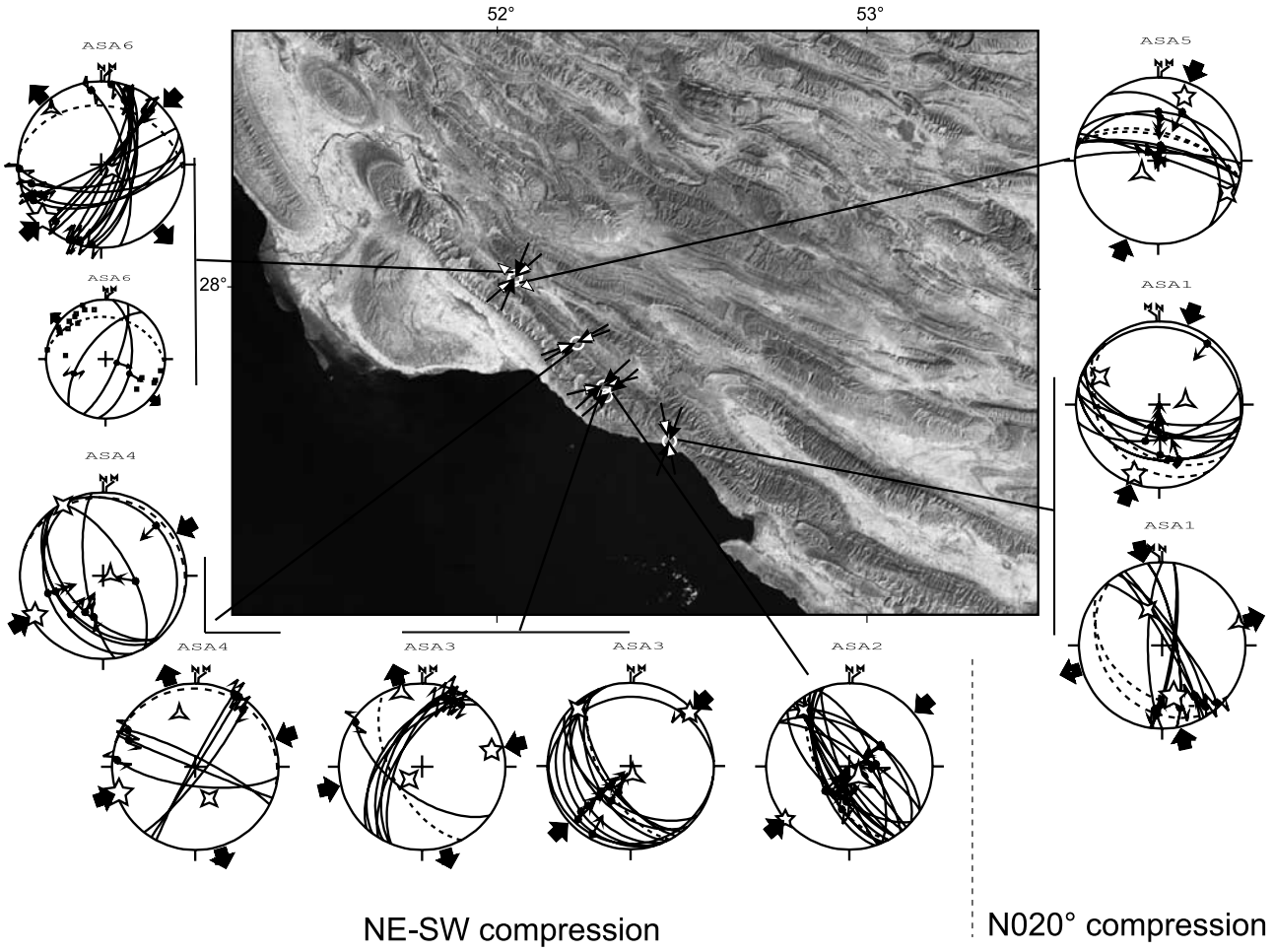

Figure 10. Faulting related to successive (left) NE-SW and (right) N020° compressional trends in the southern part of the investigated area. For arrows and diagrams, key is same as in Figures 7 and 9.

inversion, because nodal planes were not mutually perpendicular for 23 of these earthquakes. For the remaining data set, the inversion process accounts for 44 focal mechanisms, 6 earthquakes being rejected. The tensor solution is stable in terms of stress axes and Φ ratio; it is obtained from a ω_{ACC} value of 65% and corresponds to a σ_1 axis oriented N206° (±5) (Figure 12b) and a highly plunging σ_2 axis (096 69). The calculated Φ value is 0.13 (within a possible range 0–0.3). This N206° direction of compression is consistent with the mean direction of the P axes deduced from microearthquakes whatever the type of focal mechanisms (reverse or strike-slip) (Figure 13).

[33] The inversion process reveals that the focal mechanisms of small and moderate earthquakes are consistent in the area of interest. With both sets the σ_1 axes are tightly constrained around the N205° azimuth, whereas the σ_2 and σ_3 axes are not well defined in the plane perpendicular to σ_1, suggesting likely stress permutations. This compressional/strike-slip stress regime accounts for the coeval occurrence of reverse and strike-slip faulting whatever earthquake magnitudes. The good fit of focal mechanisms of earthquakes shallower than 8 km with this solution supports that despite the likely role of mechanical boundary played by the Hormuz evaporites, the current state of stress is probably similar in the cover and the basement.

[34] The computed N020–030° compressional trend is in good agreement with the pattern and kinematics of active faults in the western Fars [*Baker et al.*, 1993; *Berberian*, 1995; *Bachmanov et al.*, 2004]. These active faults include the Kazerun-Borazjan and Karebass right-lateral strike-slip faults as well as the N010 to N025 trending Quaternary and still active normal faults bounding the Dasht-e-Arjan graben (Figure 14). These normal faults display a clear geomorphic signature and cut through the Zagros folds; such normal

Figure 9. Faulting related to successive (a) NE-SW and (b) N020° compressional trends in the northern part of the investigated area: 1, reverse faulting regime (σ_3 vertical); 2, strike-slip faulting regime (σ_2 vertical); 3, normal faulting regime (σ_1 vertical). For diagrams, key is same as in Figure 7.

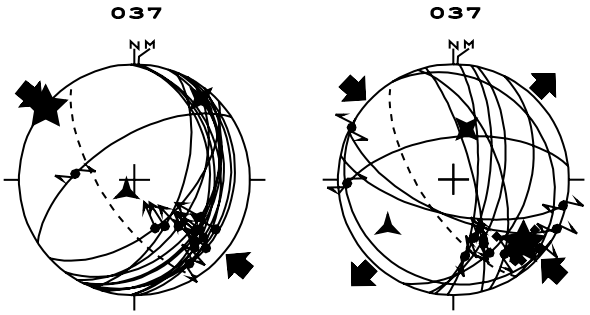

Figure 11. Example of faulting related to the N120° compressional trends. Key is same as in Figure 7.

faulting may occur in local settings such as releasing bends or extensional relays of strike-slip faults (such as the Karebass fault), under a σ_3 axis being horizontal and trending N110°, i.e., subperpendicular to the regional compression.

5.2. Cenozoic Faulting and Stress Regimes in the Western Fars

5.2.1. Modes and Conditions of Mesoscale Brittle Faulting Within the Fars Cover

[35] Mesoscale faulting (and bedding-parallel slip) observed in the field is associated with shear calcite fibers (and even gypsum fibers in local evaporite facies from Gachsaran Formation (Figure 7b) and Agha Jari Formation (Figure 7d)). In addition, pervasive pressure solution accompanied faulting as evidenced by widespread stylolitization. We conclude that the rocks investigated (mainly) deformed within the elastic-frictional regime. Hydraulic breccia in some sites additionally indicate local high fluid pressures may have prevailed during faulting.

[36] Faulting conditions in the cover can be further constrained by examination of modes on internal deformation of limestones. Analysis of calcite twin strain has been carried out from limestones from the Pabdeh-Gurpi Formations, Asmari-Jahrom Formation, Champeh Member of the Gachsaran Formation and Mishan Formation [*Dissez*, 2004; *Amrouch*, 2005]. In both the matrix and the veins

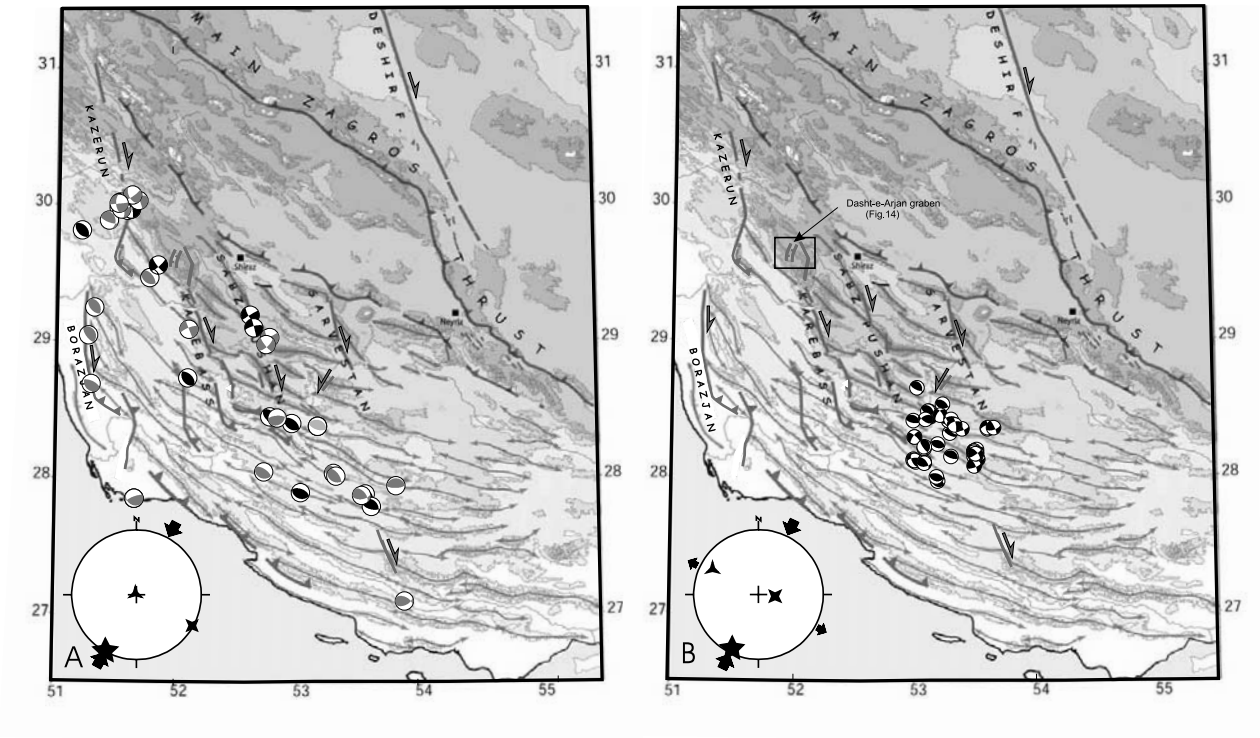

Figure 12. Earthquake focal mechanisms and related present-day principal stress axes derived from inversion. Diagrams with stars indicate stress axes with five points (σ_1), four points (σ_2), and three points (σ_3). For geological background, see Figure 3b. (a) Focal mechanisms of moderate earthquakes reported by *Talebian and Jackson* [2004] (see Table 1). These focal mechanisms include mechanisms constrained by *P* and *SH* body wave modeling (first-motion compressional quadrant in black), Harvard CMT solutions (first-motion compressional quadrant in dark grey) and first motion fault plane solutions (first-motion compressional quadrant in light grey). (b) Focal mechanisms of relocated microearthquakes reported by *Tatar et al.* [2004] (see Table 2).

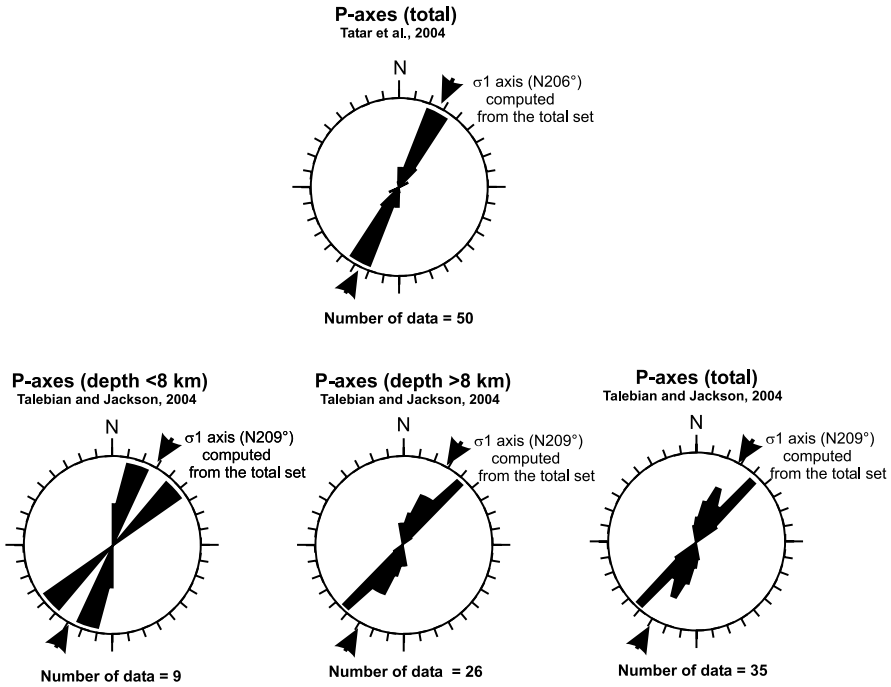

Figure 13. Rose diagrams of orientations of *P* axes for microearthquakes [*Tatar et al.*, 2004] and moderate earthquakes [*Talebian and Jackson*, 2004]. The directions of the σ_1 axes computed from inversion of focal mechanisms are reported for comparison. Note the overall consistency of *P* axes of moderate earthquakes occurring at depth shallower than 8 km (possible cover earthquakes) and at depth greater than 8 km (basement earthquakes).

deformation occurred under a thin-twin regime, suggesting that temperature remained lower than 150°–200°C [e.g., *Ferrill et al.*, 2004] and that internal strain by twinning did not exceed 3–4%.

5.2.2. Late Cenozoic Stress Regimes

5.2.2.1. Faulting Related to NE-SW Compression

[37] The first faulting event is marked by reverse and strike-slip faults and is related to a compressional trend striking NE-SW on average (Figure 9a). When bed tilting is sufficiently steep to prevent uncertainties, it can be unambiguously identified as having prevailed mainly before folding (e.g., Figures 8b and 9, site 047), but also sometimes during (e.g., Figure 9, sites 034 and 045) and after folding (e.g., Figure 10, site ASA3). Even though these observations were not made all together in individual sites, this compression is therefore clearly associated with the main folding phase at the regional scale. Normal faults associated with strike-slip faults indicate a component of perpendicular coeval horizontal extension (Figure 9, sites 047 and 059).

[38] The departure from the mean NE-SW compression is sometimes large in some sites. However, the NE-SW compressional trend is parallel to the shortening direction inferred from analyses of magnetic fabrics within Cenozoic sandstones in the same area [*Bakhtari et al.*, 1998] (Figure 15).

5.2.2.2. Faulting Related to N020° Compression

[39] A more recent faulting event related to a N020° compression can be distinguished from the previous NE-SW compression (Figure 9b). In sites where both compression have been recognized (e.g., site 047, Figure 8a), superimposed striations on fault surfaces and considerations of fault versus bedding attitudes suggest that the N020° compression-related faulting episode postdates that related to the NE-SW compression. For instance, some NE-SW trending strike-slip faults in site 047 show two striations, the horizontal ones indicating left-lateral motion cutting the NE dipping ones consistent with right-lateral motion. Additionally, the latter lie within the bedding as the σ_1 and σ_3 axes of the computed stress tensor, while σ_2 axis is perpendicular to bedding (Figure 8a). This unambiguously suggests that faulting related to the NE-SW compression occurred first, mainly before local folding, and must be interpreted as the earliest event. It clearly predates fault development related to the N020° compression which clearly occurred after folding. In most sites, faulting related to the N020° compression postdates folding (e.g., Figure 9b, sites 40, 44 and 47). Some observations (e.g., site 035) however suggest that folding may have (at least locally) continued and probably ended during this faulting event. The N020° compression is associated with subperpendicular extension marked by N-S to N020° trending normal faults (Figure 9, site 041).

[40] It is sometimes difficult to clearly attribute local compressional trends to either the NE-SW or the N020° compression on the basis of the only directional consistency. This criterion is in most cases reliable, but may fail when a single compressional trend is recognized and when this

Figure 14. Dasht-e-Arjan graben and its bounding active normal faults from Landsat image. Location is indicated on Figure 12b.

trend is intermediate between NE-SW (even ENE-WSW) and N020° (Figure 15). In addition, fold trends evolve progressively from NW-SE to E-W from the western to the eastern part of the area investigated. Consequently, attributing a local compressional trend to the NE-SW or the N020° regime may be in some cases ambiguous. For instance, in the site 045, the N217° oriented compression typically shows an intermediate trend between the NE-SW (N040–050°) and the N020° trends. We have chosen to relate this trend to the NE-SW regime (see Figure 9a) mainly on the basis on the attitude of the stress axes with respect to bedding. Striations on faults as well as the computed σ_1 axis are not horizontal but are dipping less than the bedding, indicating synfolding horizontal compression and related faulting. Since the NE-SW has been recognized as the regime prevailing mainly before and during folding, the N217° trend has been related to this regime. Along the Kazerun segment of the KBF, *Authemayou et al.* [2005] identified a compressional/strike-slip regime with a single N035–040° compressional

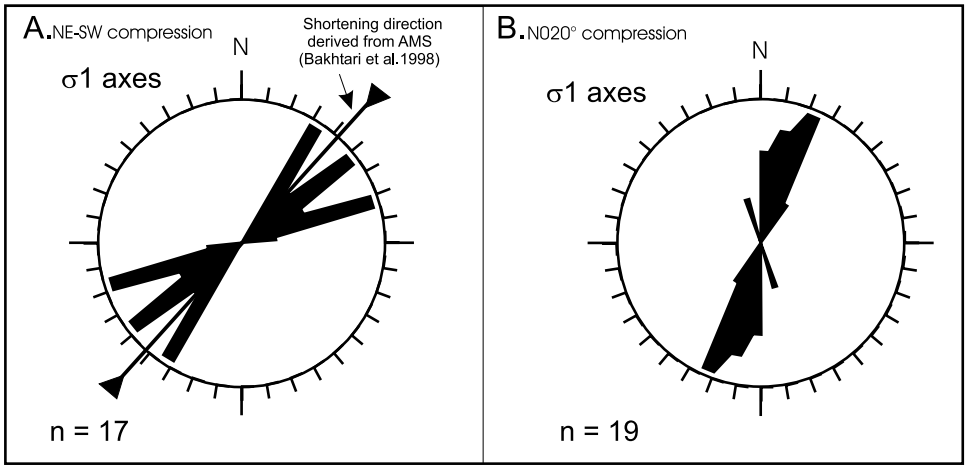

Figure 15. Rose diagrams showing the orientations of the local σ_1 axes deduced from microtectonic measurements discussed in this paper for (a) NE-SW compression and (b) N020° compression. In Figure 15a the mean shortening directions deduced from AMS studies in the same area have also been reported [*Bakhtari et al.*, 1998]. The "n" value indicates the number of σ_1 axes reported on the rose diagrams.

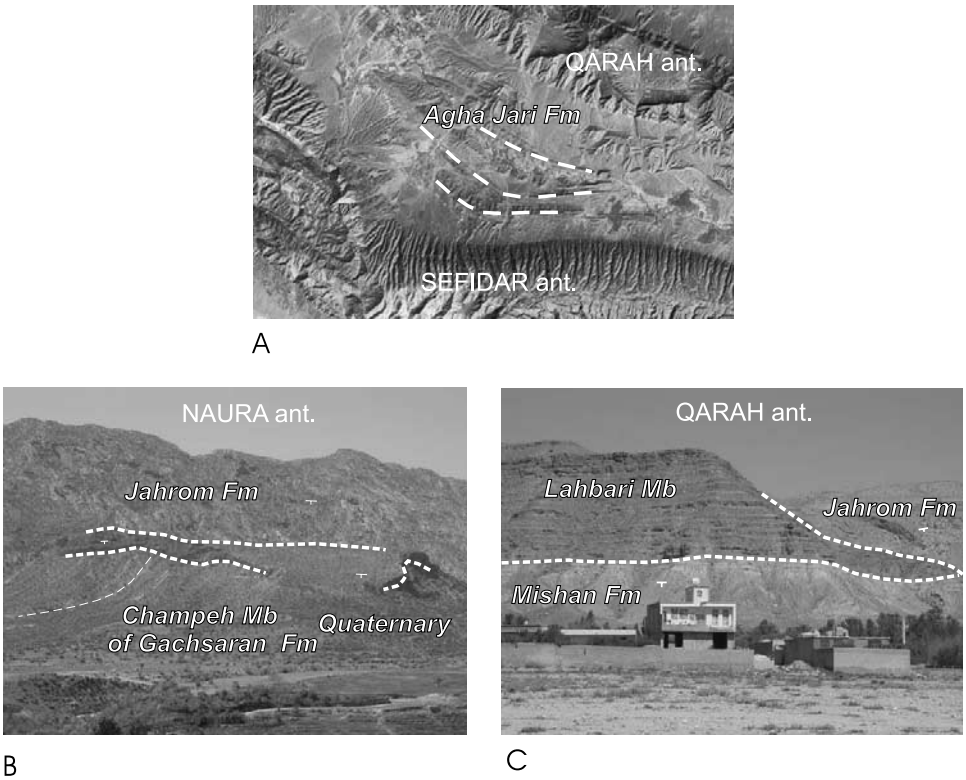

Figure 16. Dating of the main phase of folding in the western Fars. (a) Progressive unconformities in the Agha Jari Formation seen on the Landsat TM image south of Qarah anticline. (b) Unconformable attitude of the fluvial deposits of presumable Quaternary age above the Champeh Member of Gachsaran Formation north of the Naura anticline. (c) Unconformable attitude of the equivalent of the Plio-Pleistocene Bakhtyari Formation above the Mishan Formation south of the Qarah anticline.

trend, while the compression is rather nearly N-S in the bended northernmost part of the KBF connecting to the MRF. Such an occurrence of intermediate compressional trends may suggest a progressive change from NE-SW to N020° compression, a transition consistent with the scenario involving progressive late/post folding vertical axis clockwise block rotations (see section 6).

5.2.2.3. Enigmatic N120° Compression

[41] A late faulting episode related to a fold axis parallel N120° compression has also been identified (Figure 11). Attitude of related faults suggests that this compression generally postdates folding (Figures 8b and 8c). In contrast to the other events, it has been clearly identified only in sites located close to or within fault zones, between the Karebass and Sabz-Pushan fault zones (sites 035, 037 and 044) or suspected in the vicinity of the Sarvestan fault (site 065).

5.3. Dating of Deformation and Related Stress Regimes

[42] The fault populations formed under the NE-SW and the N020° compressions (Figures 9 and 10) have been recognized in the different formations analyzed regardless of their age, suggesting that they are younger than the youngest faulted rocks (i.e., middle Miocene Mishan Formation). Since the two compressions succeeded during and after folding, dating the stress regimes requires dating of folding.

[43] At the scale of the Zagros, folding mostly took place during the deposition of the upper part of the late Miocene-Pliocene Agha Jari Formation, and before the deposition of the unconformable Bakhtyari conglomerates [e.g., *Hessami et al.*, 2001]. In the area investigated, between Qarah and Sefidar anticlines, the highly dipping Jahrom, Mishan, and Agha Jari formations are unconformably overlain by fluvial deposits equivalent to the Plio-Pleistocene Bakhtyari Formation. (Figure 16c). Between Naura-Meymand and Sim anticlines, the Asmari-Jahrom Formations and Champeh Member are again unconformably overlain by fluvial deposits of probable Quaternary age (Figure 16b). This confirms that the main phase of folding had ended by then. Figure 16a suggests occurrence of progressive unconformities (growth strata) within the Agha Jari syncline south of the Qarah anticline. Our observations therefore corroborate a likely ~5 Ma age for the main phase of folding in the Fars (Figure 17) depending on the current uncertainties on the age of the top of the Agha Jari Formation and of Bakhtyari Formation.

[44] Such unconformities therefore testify for a nearly coeval activity of folds in the late Miocene-Pliocene all over the range. Note however that this does not imply that deformation did not propagate toward the external parts of the range, as commonly observed in thrust wedges. A way to explain that the main folding phase began everywhere at

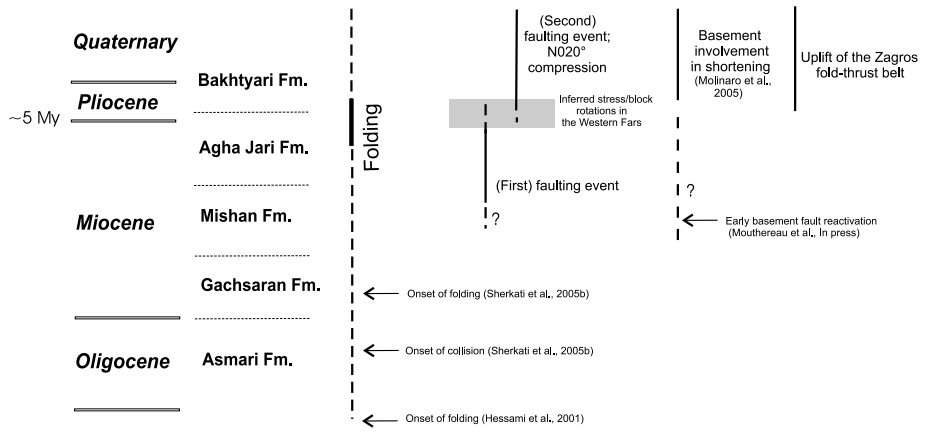

Figure 17. Summary of the proposed time occurrence of folding, block rotations, basement thrusting, and regional uplift in the western Fars area.

the end of Miocene is that the Hormuz basal decollement was simultaneously active at that time over a wide area, in agreement with the very rapid propagation of deformation above weak decollement horizons shown by analogue models [e.g., *Letouzey et al.*, 1995; *Cotton and Koyi*, 2000; *Costa and Vendeville*, 2002]. Thrusting and folding occurred earlier in the Imbricate Zone [e.g., *Hessami et al.*, 2001; *Molinaro et al.*, 2005], supporting southward migration of deformation. Furthermore, the overall southward migration through time of the flexural troughs and related depocenters derived from isopach maps [*Motiei*, 1993] supports a consistent southward propagation through time of orogenic loading and of related foredeep.

[45] Local tilting of the Bakhtyari conglomerates and of its time equivalent (Figure 16b) throughout the Zagros [e.g., *Hessami et al.*, 2001] suggests recent, although limited, folding. Basement seismicity and shortening derived from GPS, together with active folding observed near the mountain front [*Mann and Vita-Finzi*, 1988], reflects still ongoing shortening in the outer part of the Zagros wedge.

[46] Because the NE-SW compression prevailed before (and during) folding while the N020° compression mainly occurred as a posttilting regime, the change in compressional trend likely occurred during the late stages of the main Mio-Pliocene phase of folding (Figure 17). The late N020° compression still prevails at the present-day; it is consistent with dextral motions along Quaternary N-S trending faults in the Zagros [e.g., *Bachmanov et al.*, 2004] and with the N020–030° present-day compressional trend deduced from seismicity (this study).

6. Discussion and Conclusions

6.1. Local Versus Regional Significance of Successive Stress Regimes

[47] In this section we aim at discussing whether the reconstructed late Cenozoic stress regimes can help us to understand the regional tectonic evolution of the domain investigated. The stress regimes identified from fault slip data inversion may have either a local or a regional significance, and only those representative at a large scale have the potential to bring constraints on the regional tectonic evolution. We assume that only those unambiguously recognized throughout the entire area may have a regional meaning. The other ones likely reflect local effects and should not be taken into account at the regional scale. Among the successive stress regimes reported only the NE-SW and the N020° compressional trends have been identified unambiguously over the area investigated, so only both will be considered hereinafter. Note that we can rule out that these two trends only reflect dispersion on the basis of both their regional directional consistency and unambiguous relative chronology observations supporting separation where these trends were identified in the same sites.

[48] We have plotted the convergence vector of Arabia with respect to Eurasia computed from GPS sites of *Vernant et al.* [2004], and the geological motion over the last 3 Myr derived from combination of the Nubia/Eurasia motion according to *Calais et al.* [2003] and of the Nubia/Arabia motion from *Chu and Gordon* [1998] (Figure 18). These motions are compared to the average motion of Arabia with respect to Eurasia since 10.6 Ma from *McQuarrie et al.* [2003] (Figure 18). Comparison of these motions suggest that although the Arabia-Eurasia motion derived from geodesy is slightly lower and rotated counterclockwise with respect to the motion over the last 3 Myr, the overall convergence of Arabia toward Eurasia did not change during the late Cenozoic, especially since the onset of major fold development in the Fars area (about 5 Ma). As a consequence, the change in compressional trends identified from tectonic analyses cannot be related to a change in plate kinematics over the time span considered. This change in compressional trends should better be regarded as reflecting the local structural evolution of the belt and reorganization of deformation zones within the framework of the Arabia-Eurasia convergence.

[49] The occurrence of two regionally significant but distinct compressional trends throughout the investigated area, namely NE-SW and N020°, at least since 5 Ma,

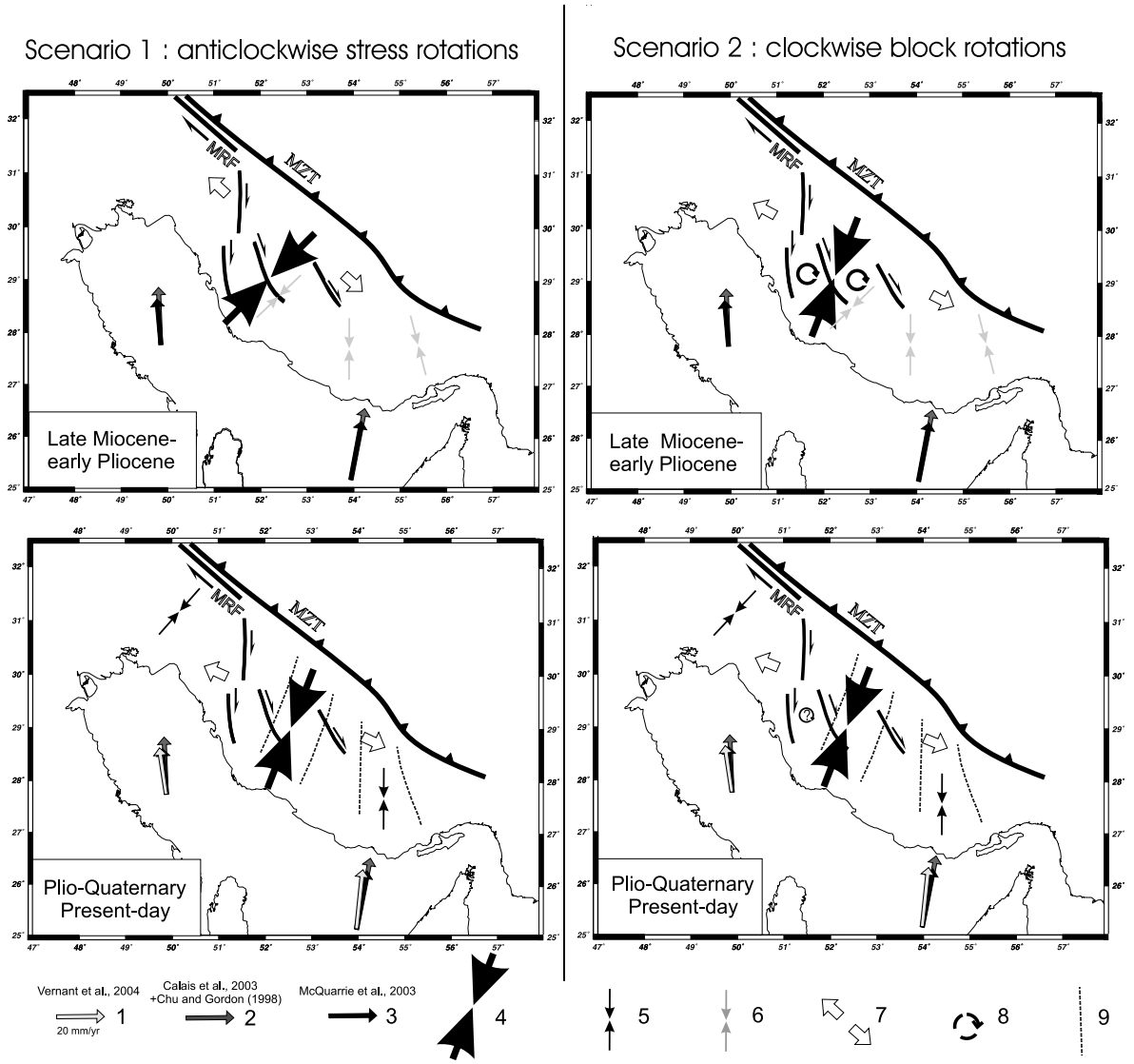

Figure 18. Possible scenarios of tectonic evolution of the western Fars area since the early Miocene: 1, Arabia-Eurasia convergence vector after *Vernant et al.* [2004]; 2, Arabia-Eurasia convergence vector over the last 3 Myr derived from combination of the Nubia/Eurasia motion according to *Calais et al.* [2003] and of the Nubia/Arabia motion from *Chu and Gordon* [1998]; 3, average motion of Arabia with respect to Eurasia since magnetic anomaly 5 (10.6 Ma) from *McQuarrie et al.* [2003]; 4, direction of paleostress/stress deduced from this study; 5, compressional trend after *Talebian and Jackson* [2004]; 6, shortening from AMS after *Bakhtari et al.* [1998]; 7, regional extension (this study); 8, block rotations inferred from this study; 9, first-order stress/shortening trajectories within the Fars arc.

deserves consideration. Two possible scenarios may explain this apparent complexity. Scenario 1 involves regional stress deviations related to the inherited fault pattern, while scenario 2 involves cover (crustal ?) block rotations within the Kazerun/Karebass/Sabz Pushan strike-slip fault system (Figure 18).

[50] In scenario 1, a NE-SW compression prevailed from the early middle Miocene to the late stages of the main phase of fold development. In the absence of significant block rotations, this compressional trend, oblique to the nearly N-S convergence vector, could result from deviations in the cover of the regional compression due to the inherited basement fault network, i.e., the pattern of N-S transcurrent faults of the western Fars. This compressional trend oblique at high angle to the faults is in good agreement with the development of N150° trending folds parallel to these fault zones (e.g., Qazi anticline parallel to the Sarvestan fault) suggesting a noticeable amount of fault-perpendicular shortening. This compression prevailed before and during the main phase of fold development. It was followed by late

folding under a still currently prevailing N020° compression consistent with right-lateral wrench movements along Kazerun/Karebass/Sarvestan strike-slip faults cutting, dragging and offsetting previously formed folds.

[51] In scenario 2, the apparent change of the compressional trend from NE-SW to N020° through time is related to progressive vertical axis clockwise rotations of cover blocks in relation to right-lateral wrench deformation accommodated by the Kazerun/Karebass/Sabz Pushan fault system. In this scenario, the compression/shortening direction remained more or less N020° from the middle-late Miocene to present-day in this part of the Zagros. Occurrence of compressional trends intermediate between NE-SW and N020° support such progressive block rotations.

[52] The possible clockwise block rotations are consistent with the slight change of the mean fold trend within the Kazerun/Karebass/Sabz-Pushan fault system. The mean fold trend evolves from N130° to the NW and to the north of the studied area to locally N140°–150° within the fault system (Figure 3). Although this trend evolution basically reflects curvature of the Fars arc, it is consistent with the clockwise block rotations inferred from the succession of compressional trends. This relationship between rotation of compressional trend and of fold axes is further supported by the identification of only the N020° compression before and after folding in the site 075 north of Shiraz (Figure 7e) where folds trend N110–120°. This site is located outside the KBF-Sarvestan corridor (Figure 5) and therefore should not have undergone clockwise rotation if our scenario 2 is plausible.

[53] The rotations invoked in scenario 2 are consistent with the clockwise rotations suggested by AMS studies to explain the systematic anticlockwise obliquity between the prefolding magnetic lineation and the fold axes [*Bakhtari et al.*, 1998]. *Aubourg et al.* [2004] also consider that contrasting patterns of early AMS shortening directions and of *P* axes of earthquakes can be accounted for by a longer deformation history recorded by AMS including vertical axis rotations. *Molinaro et al.* [2005] recently included such clockwise rotations for the western Fars in their tectonic model. These rotations are however not consistent with anticlockwise rotations around vertical axis of Kazerun/Karebass/Sabz Pushan and Sarvestan faults as implied by the model of *Talebian and Jackson* [2004]. Unfortunately, available paleomagnetic data show local unconsistent clockwise and anticlockwise rotations and are therefore currently unable to unambiguously discriminate between the different models (C. Aubourg, personal communication, 2005).

[54] An interesting point is that, in scenario 1, the N020° compressional trend more or less prevailed since the onset of the main phase of basement-involved shortening [e.g., *Molinaro et al.*, 2005], even though early localized basement thrusting (early basement fault reactivation?) is strongly suspected since the middle Miocene [*Mouthereau et al.*, 2005]. Basement-involved shortening is still active, especially in the outer part of the wedge, as indicated by basement seismicity, and the main phase of folding of the detached sedimentary cover has probably ceased by now. This may explain the good consistency of the N020° compressional trend derived from (Mio)-Pliocene microfaulting observed in the cover after folding with the N020–030° present-day compressional trend derived from inversion of focal mechanisms of basement earthquakes; decoupling by the Hormuz salt being presumably less efficient during basement-involved shortening (thick-skinned deformation stage) compared with the previous thin-skinned deformation stage.

[55] A similar situation, with present-day basement-involved shortening and consistent deep (basement) and near-surface (cover) stresses despite a major decollement level at the base of the cover, occurs in the Jura Mountain [e.g., *Becker*, 1999; *Lacombe and Mouthereau*, 2002]. This arcuate belt was formed during the Mio-Pliocene in the western Alpine foreland in response to folding and faulting of the Mesozoic cover detached from the underlying basement above the late Triassic evaporites. Seismotectonic analyses as well as in situ stress measurements support that a structural deformation mode with basement-involved shortening prevails today in the southeastern Jura belt. Contemporary near-surface stress data do not agree with paleostress orientations related to Jura emplacement as deduced from fault slip data [*Homberg et al.*, 1999]. Moreover, stress provinces defined on the basis of homogeneous maximum horizontal stress orientations in the Jura Mountains extend far into the nondetached foreland, without signs of variations across the border between the folded Jura and its undeformed foreland. These results together suggest that active thin-skinned tectonics for the Jura Mountains has ceased [*Becker*, 1999]. Seismicity further testifies deep basement tectonics and strongly suggests deep-seated thrusting in the entire internal Jura-Molasse basin domain. Earthquakes hypocenters are distributed throughout the entire depth range of the crust down to 30 km. Earthquakes above and below the decollement horizon show similar focal mechanisms, which are in good agreement with present-day in situ stresses in the southern Jura area [*Becker*, 1999]. This indicates stress orientations similar in the cover rocks and in the basement. Like in the Zagros, the similarity between deep and near-surface stresses, the rapid uplift of the southern internal Jura as well as crustal seismicity reflect present-day active tectonics involving the basement below the main Triassic decollement level in the Molasse basin and the southern Jura mountains [*Lacombe and Mouthereau*, 2002].

[56] Within the tectonic and kinematic framework of the Zagros described above, the N120° compression is enigmatic. A possible explanation could have been that it corresponds to a late compression responsible for the development of NE-SW trending folds as suggested by *Ricou* [1976], causing refolding of earlier NW-SE trending folds. This however seems to be difficult to reconcile with the trend of the Arabia-Eurasia convergence over the last 10 Myr. Furthermore, this compressional trend has been recognized only in the close vicinity of the strike-slip fault zones. For this reason and because the N110–120° compression trends nearly perpendicular to the N020° compression, a possible explanation consists of a stress permutation, a common feature in brittle tectonics [*Hu and Angelier*,

2004]. Alternatively, this N120° compression could correspond to a significant but minor tectonic signal. The question of the significance of this event, either it is regional or local, remains still open.

6.2. Significance of Transverse Structures: Strike-Slip Versus Transfer Faulting

[57] Experimental and analytical modelings coupled with field observations have resulted in a better understanding of the geometry and mechanism of transverse zones [e.g., *Apotria et al.*, 1992; *Calassou et al.*, 1993; *Philippe*, 1995; *Baby et al.*, 1994; *Apotria*, 1995]. Such domains are characterized by structures oblique to the belt. Sandbox modeling revealed that a thrust sheet moving over a décollement level may exhibit development of transverse structures in response to a lateral change in cover thickness due to basement geometry or basin boundary or to the lateral termination of the main décollement surface, which can be viewed as a high/1ow friction boundary [e.g., *Cotton and Koyi*, 2000]. A primary tear (or transfer) fault may thus appear in the cover above the decollement contemporaneously with fold-thrust development and be associated with a curvature or apparent offset of these structures as soon as they form; on both sides the amount of shortening is the same, but it may be accommodated in a different way. A primary tear fault is nearly parallel to the local transport direction. Such a system may secondarily evolve gradually into a transcurrent fault (a cover strike-slip fault), associated with a clear offset of already formed or currently forming folds. These secondary faults may be more or less oblique to shortening. On both sides of such a fault, differential displacement/shortening may be accommodated.

[58] The interpretation of the N150°E to N-S trending Kazerun-Borazjan, Karebass, Sabz Pushan, and Sarvestan faults (Figure 3) as transfer fault zones acting during folding of the cover rather than simple strike-slip faults is based on the identification of differential accommodation of shortening on both sides of the fault, as well as the sigmoidal shape of fold axes and mismatches of compressional features on both sides. Anticline axes are bent, and die out, or are offset by segments of these faults; these segments often terminate as thrusts parallel to folds in the SFB. The faults are clearly contemporaneous with folding and act as oblique, right-lateral ramps, transferring locally and accommodating shortening across the Zagros fold belt. These transfer fault zones may have initiated in the cover strata in response to local kinematic incompatibilities during compressional thin-skinned tectonics; they however more probably developed above inherited basement features (known in the Arabian shield) during Cenozoic tectonism, which may explain their poorly defined structural expression in the cover.

[59] The KBF is a typical example of such a transfer fault zone. The Zagros belt becomes wider from NW to SE along this fault zone (Figure 3). The comparison of restored transects in NW Fars and the Izeh zone (Sherkati et al., submitted manuscript, 2005) shows that shortening is not significantly different on both sides of the KBF: it amounts 50km in northwestern Fars area and 65km in the Izeh zone. This small difference in the amount of shortening cannot explain the abrupt longitudinal offset of the MFF along the KBF. In fact, shortening is unequally distributed from one side to the other of the Kazerun transfer zone, being distributed east in the Fars over a wider area than in the Dezful. Structural style also shows differences on both sides of this transfer zone. East of KBF, where Hormuz salt is the main basal décollement level, shortening is equally distributed across the belt whereas to the west, whereas the basal décollement changes to probable Lower Paleozoic shales, deformation mostly concentrated in the inner zone [*Sherkati and Letouzey*, 2004]. As a result, there is no evidence for large (140–150 km) cumulative right-lateral strike-slip offset along the KBF as suggested by *Berberian* [1995]. Basically, the KBF should rather be viewed as an inherited basement fault that localized in the cover a major transfer zone between the Fars area and the central Zagros, trending subparallel to the nearly N-S convergence vector, and separating two strongly different structural domains during collisional shortening.

[60] The Karebass, Sabz Pushan, and Sarvestan faults have been described by *Berberian* [1995] as strike-slip faults on the basis of the strike-slip-type basement earthquake events along their trends as well as the related apparent lateral offsets of folds in the cover (e.g., at least 10 km and 20 km of displacement, respectively along the Karebass and Sarvestan faults). In their reconstructions, *Molinaro et al.* [2005] consider that these faults have acquired a surface expression only during the late evolution of the Zagros SFB, during the episode of basement-involved shortening. Because in their scenario folds have formed prior to any basement involvement in deformation, these faults were not active in the cover during folding. We rather propose that during folding, these fault zones behaved as local transfer fault zones, although of much less importance than the KBF, and superimposed onto long-lived (basement) features which largely controlled facies changes and paleogeographic evolution. For instance, the Sabz-Pushan Fault zone marks the limit between the Asmari Formation facies to the west and the Asmari-Jahrom Formation facies to the east [*Berberian*, 1995]. Moreover, close inspection of the Sabz Pushan fault zone indicate curvature of the Dalu-Sefidar anticline, local bend of the Meymand-Naura anticline, but disappearance of the Sim anticline west of the fault zone (Figures 5 and 9). Local balanced cross sections east and across the fault zone [*Dissez*, 2004] indicate that the same amount of shortening is accommodated by two folds to the west and distributed on three folds to the east. This means that the Sabz-Pushan fault zone did not behave as a simple strike-slip fault cutting through and offsetting previously formed folds, but rather as a primary tear fault, nearly parallel to local transport direction, and accommodating local kinematic incompatibilities in the cover. More generally, at the local scale, the sigmoidal and/or bayonet shapes of some fold axes can basically result from primary bend within tear fault zones in the cover located above inherited fault zones in the basement, rather than from secondary offsets along right-lateral strike-slip faults which should have induced bending in a sense opposite to that locally observed (e.g., Dalu-Sim-Meymand anticlines). This

may result in some obliquity of local fold trends to the regional compression/shortening, as previously noticed by *Bakhtari et al.* [1998] and *Aubourg et al.* [2004].

[61] It is clear however that in the more recent stages of deformation, the Kazerun-Borazjan, Karebass, Sabz Pushan, and Sarvestan faults zones acted as strike-slip faults in both the basement and the cover as their seismic activity and their steep en echelon segments suggest. At a more regional scale, the slight change from N130° to N140°–150° trend of folds between the KBF and the Karebass fault should be related to bend and drag in relation to right-lateral strike-slip faulting and related clockwise rotations. This late strike-slip kinematics is also accompanied by the development of pull-apart zones at extensional relays with some Hormuz salt plugs located there [*Talbot and Alavi*, 1996].

[62] It is possible that the change from tear faulting to strike-slip faulting may have been coeval with the change in the compressional trend from NE-SW to N020° (as involved in scenario 1) or with block rotations (as involved in scenario 2). In scenario 1, coupling across the fault zones in the cover, marked by the amount of fault-perpendicular shortening, has evolved and decreased with time when fault zones evolved to strike-slip faults. In scenario 2, block rotations presumably mainly occurred when faults underwent actual strike-slip displacement. The change from tear faulting to strike-slip faulting could also be more or less coeval with the onset of the main phase of basement-involved shortening. The close association of the KBF and Karebass fault with thrusts parallel to folds (Figure 2) suggests that during thick-skinned tectonics, the KBF and Karebass (basement) faults acted as lateral ramps of basement thrusts with a right-lateral component of motion (as indicated by earthquakes). At this stage, they likely propagated upward and overprinted in the overlying cover, acting as strike-slip faults mainly after folding. This scenario may explain the geometry of the Kazerun/Karebass,/Sabz Pushan and Sarvestan fault zones in the cover and their evolving behavior through time.

[63] According to *Talebian and Jackson* [2004], the Kazerun-Borazjan/Karebass/Sabz-Pushan/Sarvestan right-lateral strike-slip fault system accommodates the change in shortening modes from partitioned to the west (oblique convergence accommodated by NE-SW shortening perpendicular to the belt and right-lateral strike-slip faulting along the MRF at the rear) to nonpartitioned to the east (shortening parallel to convergence which is perpendicular to the E-W trend of the belt). This kinematic change requires extension along the strike of the belt, which can be achieved by the Kazerun-Borazjan/Karebass/Sabz-Pushan/Sarvestan faults if they rotate anticlockwise about vertical axis (if they do not rotate, they are not able to play this role). The highest elevation and deepest stratigraphic exposures of the SFB occur where the Karebass fault meets the western end of the Surmeh-Ghir thrust, the latter dying away with distance to the junction (Figure 3b). This kind of fault termination is considered by *Talebian and Jackson* [2004] as characteristics of intracontinental strike-slip faults that rotate about a vertical axis. However, as mentioned previously, these faults are still parallel to the roughly N-S preexisting basement trends known in the Qatar peninsula and the Arabian shield [*Motiei*, 1993] and from which they are likely inherited. This observation, together with our stress reconstructions supporting rather clockwise block rotations, seems to us difficult to reconcile with the anticlockwise rotations about vertical axis of these faults within a distributed strain pattern over the last 5 Myr as proposed by *Talebian and Jackson* [2004].

[64] We further propose that extension required for accommodating transition from partitioned deformation to the NW to nonpartitioned deformation to the SE could be partly accommodated by the obliquity of the Karebass, Sabz-Pushan, and Sarvestan faults which strike N150–160° and which are therefore slightly oblique to the N-S convergence vector. Extension can further be accommodated by local fold axis parallel extension marked by normal faults at different scales, including minor as well as large normal faults cutting the folds (Figures 9, 10, and 14). Note that limb-parallel extension and clockwise block rotations related to limb-parallel vertical simple shear are also required to accommodate curvature of the Fars salient, in agreement with most models of arc formation [e.g., *Hindle and Burkhard*, 1999]. The Kazerun-Borazjan/Karebass/Sabz-Pushan/Sarvestan fault system has been alternatively viewed as an orogen-scale horse-tail strike-slip fault termination which transfers and distributes orogen-parallel dextral slip achieved along the MRF into the thrusts and folds of the Zagros belt [*Authemayou et al.*, 2005].

6.3. Cenozoic Stress Fields and Accommodation of the (Slightly Oblique) Arabia-Eurasia Convergence in the Fars

[65] The main conclusion of this study is that, whatever the scenario adopted, the regional stress field did not change significantly since the main folding phase, i.e., about 5 Ma, in the western Fars. Most of the apparent complexity of the Cenozoic compressional trends may be explained either by early deviations of the regional stress field by the inherited pattern of the Kazerun-Borazdjan/Karebass/Sabz-Pushan faults, or by late vertical axis rigid clockwise block rotations along the western limb of the Fars arc compatible with the strike-slip kinematics of these faults.

[66] The kinematics of Mio-Pliocene small-scale faulting indicated by syntectonic growth calcite or gypsum fibers, although (1) observed in the cover and (2) basically different from that of the seismogenic faulting in term of the timescales involved (long-term, finite versus short-term incremental seismogenic deformation), interestingly indicate stress patterns (and regimes) nearly similar to those derived from the inversion of basement microearthquakes, especially for the late N020° compression,. Both types of data can thus be considered as reflecting the internal deformation of a prefractured crust as a whole (basement plus cover), despite the occurrence of the thick Hormuz salt layer at the base of the cover. For the moderate earthquakes, it is also noticeable that the current state of

stress deduced from inversion of focal mechanisms is well-constrained despite the variety of foci depths, i.e., in the cover and the basement. The consistency of the results of the inversion suggests that the current stress orientations are homogeneous in both the cover and the basement, and therefore that no significant change in trend in the crustal state of stress currently occurs across the Hormuz salt decoupling level.

[67] The homogeneity of the stress field since nearly 5 Ma provides direct justification that the pattern of deformation remained the same over the last 5 Myr [*Talebian and Jackson*, 2004]. This homogeneous stress field presumably prevailed in the Zagros since the major reorganization of the Arabia-Eurasia collision reported by several authors at about 3–5 Ma [e.g., *Allen et al.*, 2004]. The N020–030° compression presumably prevailed more or less since the fundamental change in the mechanism of deformation of the Zagros belt from thin-skinned tectonics to a generalized involvement of the basement in shortening [e.g., *Molinaro et al.*, 2005]; the Hormuz salt, although remaining a mechanical boundary for the upward propagation of most earthquakes [e.g., *Masson et al.*, 2005], having a much less important role as decoupling level than during the previous stage of dominant thin-skinned deformation.

[68] In most sites, compressional trends were derived from mixed sets of reverse and strike-slip faults, without clear regionalization of the two. At a larger scale, the close association of thrust and strike-slip movements is also revealed by the southern termination of these faults as thrusts within the SFB. The close association of both faulting regimes in the cover during the late Cenozoic tightly resembles the mixed reverse and strike-slip-type focal mechanisms of microearthquakes reported by *Tatar et al.* [2004] (Figure 12b). This is confirmed by the reconstitutions of reverse and wrench stress regimes and low Φ ratios computed from faults and small to moderate earthquakes sometimes close to 0, allowing both regimes to exist coevally. The mean N020° compressional trend is also very close to the direction of shortening which was measured during a GPS geodetic survey in the same area [*Tatar et al.*, 2002]. The seismic strain in the Zagros, even if its amplitude is small, is coaxial with geodetic strain, and this strain is homogeneous, compressive and oriented N010° [*Masson et al.*, 2005]. This indicates that since at least 5 Ma, the oblique Arabia-Eurasia convergence did not give rise to partitioning in the western Fars, in agreement with the termination of the MRF northwest of the area investigated [*Talebian and Jackson*, 2004], but rather that this oblique convergence is currently (and has been during the Plio-Quaternary) accommodated by distributed deformation involving both shortening and strike-slip motion throughout the cover and the basement.

[69] **Acknowledgments.** Field work was supported by the MEBE scientific program. Logistic support was provided by the Geological Survey of Iran (Tehran, Shiraz). A. Saïdi is thanked for his friendly help and support during our stay in Iran and fieldtrip. The first author warmly thanks J. Angelier for his help in performing inversion of earthquake focal mechanisms. V. Regard and an anonymous reviewer are also thanked for their constructive comments. Figures 1 and 2 were drawn using the GMT software [*Wessel and Smith*, 1998].

References

Agard, P., J. Omrani, L. Jolivet, and F. Mouthereau (2005), Convergence history across Zagros (Iran): Constraints from collisional and earlier deformation, *Int. J. Earth Sci.*, *94*, 401–419, doi:10.1007/S00531-005-0481-4.

Allen, M., J. Jackson, and R. Walker (2004), Late Cenozoic reorganization of the Arabia-Eurasia collision and the comparison of short-term and long-term deformation rates, *Tectonics*, *23*, TC2008, doi:10.1029/2003TC001530.

Amrouch, K. (2005), Quantification des orientations et des magnitudes des paléocontraintes tertiaires dans la chaîne plissée du Zagros par l'analyse des macles de la calcite: Lien avec les macrostructures: Implications géodynamiques, Master thesis, Univ. Pierre et Marie Curie (Paris 6), Paris, France.

Anderson, E. M. (1951), *The Dynamics of Faulting*, 2nd ed., 206 pp, Oliver and Boyd, White Plains, N. Y

Angelier, J. (1990), Inversion of field data in fault tectonics to obtain the regional stress: III-A new rapid direct inversion method by analytical means, *Geophys. J. Int.*, *103*, 363–376.

Angelier, J. (2002), Inversion of earthquake focal mechanisms to obtain the seismotectonic stress: IV-A new method free of choice among nodal planes, *Geophys. J. Int.*, *150*, 588–609.

Apotria, T. G. (1995), Thrust sheet rotation and out-of-plane strains associated with oblique ramps: An example from the Wyoming salient, USA, *J. Struct. Geol.*, *17*(5), 647–662.

Apotria, T. G., W. T. Snedden, J. H. Spang, and D. V. Wiltchensko (1992), Kinematic models of deformation at an oblique ramp, in *Thrust Tectonics*, edited by K. R. McClay, pp. 141–154, CRC Press, Boca Raton, Fla.

Aubourg, C., B. Smith, H. Bakhtari, N. Guya, A. Eshragi, S. Lallemant, M. Molinaro, X. Braud, and S. Delaunay (2004), Post-Miocene shortening pictured by magnetic fabric across the Zagros-Makran syntaxis (Iran), *Spec. Pap. Geol. Soc. Am.*, *383*, 17–40.

Authemayou, C., O. Bellier, D. Chardon, Z. Malekzade, and M. Abassi (2005), Role of the Kazerun fault system in active deformation of the Zagros fold-and-thrust belt (Iran), *C. R. Geosci.*, *337*, 539–545, doi:10.1016/j.crte.2004.12.007.

Baby, P., M. Specht, J. Oller, G. Montemurro, B. Colletta, and J. Letouzey (1994), The boomerang Chapare transfer zone (recent oil discovery trend in Bolivia): Structural interpretation and experimental appproach, in *Geodynamic Evolution of Sedimentary Basins*, edited by F. Roure et al., pp. 203–222, Technip, Paris.

Bachmanov, D. M., V. G. Trifonov, K. T. Hessami, A. I. Kozhurin, T. P. Ivanova, E. A. Rogozhin, M. C. Hademi, and F. H. Jamali (2004), Active faults in the Zagros and central Iran, *Tectonophysics*, *380*, 221–241.

Bahroudi, A., and H. A. Koyi (2003), Effect of spatial distribution of Hormuz salt on deformation style in the Zagros fold and thrust belt: An analogue modelling approach, *J. Geol. Soc. London*, *160*, 1–15.

Baker, C., J. Jackson, and K. Priestley (1993), Earthquakes on the Kazerun Line in the Zagros mountains of Iran: Strike-slip faulting within a fold-and-thrust belt;, *Geophys. J. Int.*, *115*, 41–61.

Bakhtari, H. R., D. Frizon de Lamotte, C. Aubourg, and J. Hassanzadeh (1998), Magnetic fabrics of Tertiary sandstones from the Arc of Fars (eastern Zagros, Iran), *Tectonophysics*, *284*, 299–316.

Bayer, R., et al. (2002), Active deformation in Zagros-Makran transition zone inferred from GPS, tectonic and seismological measurements, *Eos Trans. AGU*, *83*(47), Fall Meet., Suppl., Abstract S62B-1188.

Becker, A. (1999), The Jura mountains: An active foreland fold-and-thrust belt, *Tectonophysics*, *321*, 381–406.

Bellier, O., and M. L. Zoback (1995), Recent state of stress change in the Walker Lane zone, western Basin and Range Province, United States, *Tectonics*, *14*, 564–593.

Berberian, M. (1995), Master ''blind'' thrust faults hidden under the Zagros folds: Active basement tectonics and surface tectonics surface morphotectonics, *Tectonophysics*, *241*, 193–224.

Berberian, M., and G. C. P. King (1981), Towards a paleogeography and tectonic evolution of Iran, *Can. J. Earth Sci.*, *18*, 210–265.

Bergerat, F. (1987), Stress fields in the European platform at the time of Africa-Eurasia collision, *Tectonics*, *6*, 99–132.

Calais, E., C. DeMets, and J. M. Nocquet (2003), Evidence for a post-3.16 Ma change in Nubia-Eurasia-North America plate motions, *Earth Planet. Sci. Lett.*, *216*, 81–92.

Calassou, S., C. Larroque, and J. Malavieille (1993), Transfer zones of deformation in thrust wedges: An experimental study, *Tectonophysics*, *221*, 325–344.

Chu, D., and R. G. Gordon (1998), Current plate motions across the Red Sea, *Geophys. J. Int.*, *135*, 313–328.

Colman-Sadd, S. (1978), Fold development in Zagros simply folded belt, southwest Iran, *AAPG Bull.*, *62*, 984–1003.

Costa, E., and B. C. Vendeville (2002), Experimental insights on the geometry and kinematics of fold-and-thrust belts above weak, viscous evaporitic décollement, *J. Struct. Geol.*, *24*, 1729–1739.

Cotton, J. T., and H. A. Koyi (2000), Modeling of thrust fronts above ductile and frictional detachments; application to structures in the Salt Range and Potwar Plateau, Pakistan, *Geol. Soc. Am. Bull.*, *112*, 351–363.

DeBoisgrollier, T. (2004), Contraintes structurales et sédimentaires sur l'évolution du bassin et des déformations compressives dans le Zagros plissé, région du Fars, Master thesis, Univ. Pierre et Marie Curie (Paris 6), Paris.

DeMets, C., R. G. Gordon, D. F. Argus, and S. Stein (1990), Current plate motions, *Geophys. J. Int.*, *101*, 425–478.

Dissez, L. (2004), Cinématique et mécanismes de la déformation associés au plissement: Exemple d'un pli dans la région du Fars (Zagros iranien), Master thesis, Univ. Pierre et Marie Curie (Paris 6), Paris.

Falcon, N. (1974), Zagros mountains, Mesozoic-Cenozoic orogenic belts, in *Mesozoic Cenozoic Orogenic Belts: Data for Orogenic Studies*, collated and edited by A. M. Spencer, *Geol. Soc. Spec. Publ.*, *4*, 199–211.

Ferrill, D. A., P. Morris, M. A. Evans, M. Burkhard, R. H. Groshong, and C. M. Onasch (2004), Calcite twin morphology: A low-temperature deformation geothermometer, *J. Struct. Geol.*, *26*, 1521–1529.

Hessami, K., H. A. Koyi, C. J. Talbot, H. Tabasi, and E. Shabanian (2001), Progressive unconformities within an evolving foreland fold-thrust belt, Zagros mountains, *J. Geol. Soc. London*, *158*, 969–981.

Hindle, D., and M. Burkhard (1999), Strain, displacement and rotation associated with the formation of curvature in fold belt: the example of the Jura arc, *J. Struct. Geol.*, *21*, 1089–1101.

Homberg, C., O. Lacombe, J. Angelier, and F. Bergerat (1999), New constraints for indentation mechanisms from the Jura Mountains (France), *Geology*, *27*, 827–830.

Hu, J. C., and J. Angelier (2004), Stress permutations: Three-dimensional distinct element analysis accounts for a common phenomenon in brittle tectonics, *J. Geophys. Res.*, *109*, B09403, doi:10.1029/2003JB002616.

Jackson, J., and D. McKenzie (1984), Active tectonics of the Alpine-Himalayan belt between western Turkey and Pakistan, *Geophys. J. R. Astron. Soc.*, *64*, 561–586.

Jackson, J., and D. McKenzie (1988), The relationship between plate motions and seismic tensors, and the rates of active deformation in the Mediterranean and Middle East, *Geophys. J. R. Astron. Soc.*, *93*, 45–73.

Jackson, J. A. (1980), Reactivation of basement faults and crustal shortening in orogenic belts, *Nature*, *283*, 343–346.

Jackson, J. A., and T. Fitch (1981), Basement faulting and the focal depths of the larger earthquakes in the Zagros mountains, Iran, *Geophys. J. R. Astron. Soc.*, *64*, 561–586.

Lacombe, O., and F. Mouthereau (2002), Basement-involved shortening and deep detachment tectonics in forelands of orogens: Insights from recent collision belts (Taiwan, Western Alps, Pyrenees), *Tectonics*, *21*(4), 1030, doi:10.1029/2001TC901018.

Lacombe, O., J. Angelier, P. Laurent, F. Bergerat, and C. Tourneret (1990), Joint analyses of calcite twins and fault slips as a key for deciphering polyphase tectonics: Burgundy as a case study, *Tectonophysics*, *182*, 279–300.

Letouzey, J. (1986), Cenozoic paleo-stress pattern in the Alpine foreland and structural interpretation in a platform basin, *Tectonophysics*, *132*, 215–231.

Letouzey, J., and S. Sherkati (2004), Salt movement, tectonic events, and structural style in the central Zagros fold and thrust belt (Iran), paper presented at Salt Sediments Interactions and Hydrocarbon Prospectivity: Concepts, Applications, and Case Studies for the 21st Century, 24th Bob F. Perkins Research Conference, article Gulf Coast Sect., Soc. Sediment. Geol., Houston, Tex.

Letouzey, J., B. Colletta, R. Vially, and J. C. Chermette (1995), Evolution of salt-related structures in compressional settings, in *Salt Tectonics: A Global Perspective*, edited by M. P. A. Jackson, D. G. Roberts, and S. Snelson, *AAPG Mem.*, *65*, 41–60.

Letouzey, J., S. Sherkati, J. M. Mengus, H. Motiei, M. Ehsani, A. Ahmadnia, and J. L. Rudkiewicz (2002), A regional structural interpretation of the Zagros mountain belt in northern Fars and high Zagros (SW Iran), paper presented at AAPG Annual Meeting 2002, Houston, Tex.

Macedo, J., and S. Marshak (1999), Controls on the geometry of fold-thrust belt salients, *Geol. Soc. Am. Bull.*, *111*, 1808–1822.

Maggi, A., J. A. Jackson, K. Priestley, and C. Baker (2000), A re-assessment of focal depth distributions in southern Iran, the Tien Shan and northern India: Do earthquakes really occur in the continental mantle?, *Geophys. J. Int.*, *143*, 629–661.

Mann, C. D., and C. Vita-Finzi (1988), Holocene serial folding in the Zagros, in *Gondwana and Tethys*, edited by M. G. Audley-Charles and A. Hallam, *Geol. Soc. Spec. Publ.*, *37*, 51–59.

Masson, F., J. Chéry, J. Martinod, D. Hatzfeld, P. Vernant, F. Tavakoli, and M. Ghafory-Ashtiani (2005), Seismic versus aseismic deformation in Iran inferred from earthquakes and geodetic data, *Geophys. J. Int.*, *160*(1), 217, doi:10.1111/j.1365-246X.2004.02465.x.

McCall, G. J. H. (1997), The geotectonic history of the Makran and adjacent areas of southern Iran, *J. Asian Sci.*, *15*, 517–531.

McClusky, S., et al. (2000), Global Positioning System constraints on plate kinematics and dynamics in the eastern Mediterranean and Caucasus, *J. Geophys. Res.*, *105*, 5695–5719.

McClusky, S. M., R. Reillinger, S. Mahmoud, D. Ben Sari, and A. Tealeb (2003), GPS constraints on Africa (Nubia) and Arabia plate motions, *Geophys. J. Int.*, *155*, 126–138.

McKenzie, D. (1972), Active tectonics of the Mediterranean region, *Geophys. J. R. Astron. Soc.*, *30*, 109–185.

McKenzie, D. (1978), Active tectonics of the Alpine-Himalayan belt: The Aegean Sea and surrounding regions, *Geophys. J. R. Astron. Soc.*, *55*, 217–254.

McQuarrie, N. (2004), Crustal scale geometry of the Zagros fold-thrust belt, Iran, *J. Struct. Geol.*, *26*, 519–535.

McQuarrie, N., J. M. Stock, C. Verdel, and B. P. Wernicke (2003), Cenozoic evolution of Neotethys and implications for the causes of plate motions, *Geophys. Res. Lett.*, *30*(20), 2036, doi:10.1029/2003GL017992.

Molinaro, M., P. Leturmy, J.-C. Guezou, D. Frizon de Lamotte, and S. A. Eshraghi (2005), The structure and kinematics of the southeastern Zagros fold-thrust belt, Iran: From thin-skinned to thick-skinned tectonics, *Tectonics*, *24*, TC3007, doi:10.1029/2004TC001633.

Morris, P. (1977), Basement structure as suggested by aeromagnetic surveys in southwest ran, paper presented at Second Geological Symposium of Iran, Iranian Pet. Inst., Oil Serv. Co. Iran, Tehran.

Motiei, H. (1993), *Geology of Iran: Stratigraphy of Zagros*, 536 pp., Geol. Surv. of Iran, Tehran.

Mouthereau, F., O. Lacombe, and B. Meyer (2005), The Zagros folded belt (Fars, Iran): Constraints from topography and critical wedge modelling, *Geophys. J. Int.*, in press.

O'Brien, C. A. E. (1957), Salt diapirism in south Persia, *Geol. Mijnbouw*, *19*, 357–376.

Onasch, C. M. (1983), Dynamic analysis of rough cleavage in the Martisburg Formation, Maryland, *J. Struct. Geol.*, *5*, 73–82.

Ozden, S., S. Over, and U. C. Unlungenc (2002), Quaternary stress regime change along the eastern North Anatolian fault zone, Turkey, *Int. Geol. Rev.*, *44*, 1037–1052.

Philippe, Y. (1995), Rampes latérales et zones de transfert dans les chaînes plissées: Géométrie, conditions de formation et pièges structuraux associés, these, Univ. de Savoie, Chambery, France.

Regard, V., O. Bellier, J. C. Thomas, M. R. Abbassi, J. Mercier, E. Shabanian, K. Feghhi, and S. Soleymani (2004), Accommodation of Arabia-Eurasia convergence in the Zagros-Makran transfer zone, SE Iran: A transition between collision and subduction through a young deforming system, *Tectonics*, *23*, TC4007, doi:10.1029/2003TC001599.

Ricou, L. E. (1976), Evolution structurale des Zagrides, la region clef de Neyriz (Zagros iranien), *Mem. Soc. Geol. Fr.*, *125*, 1–144.

Sattarzadeh, Y., J. W. Cosgrove, and C. Vita-Finzi (2000), The interplay of faulting and folding during the evolution of the Zagros deformation belt; in *Forced Folds and Fractures*, edited by J. W. Cosgrove and M. S. Ameen, *Geol. Soc. Spec. Publ.*, *169*, 187–196.

Sengör, A. M. C., N. Görür, and F. Saroglu (1985), Strike-slip faulting and related basin formation in zones of tectonic escape: Turkey as a case study, in Strike-Slip Faulting and Basin Formation, edited by K. T. Biddle and N. Christie-Blick, *Spec. Publ. Soc. Econ. Paleontol. Mineral.*, *37*, 227–264.

Sepehr, M., and J. W. Cosgrove (2004), Structural framework of the Zagros fold-thrust belt Iran, *Mar. Pet. Geol.*, *21*, 829–843.

Sepehr, M., and J. W. Cosgrove (2005), Role of the Kazerun Fault Zone in the formation and deformation of the Zagros fold-thrust belt, Iran, *Tectonics*, *24*, TC5005, doi:10.1029/2004TC001725.

Sherkati, S. (2004), Style tectonique et cinématique du plissement dans le Zagros iranien (zone d'Izeh): Conséquences pétrolières, Ph.D. thesis, Univ. de Cergy-Pontoise, Cergy-Pontoise, France.

Sherkati, S., and J. Letouzey (2004), Variation of structural style and basin evolution in the central Zagros (Izeh zone and Dezful Embayment), Iran, *Mar. Pet. Geol.*, *21*, 535–554.

Sherkati, S., M. Molinaro, D. Frizon de Lamotte, and J. Letouzey (2005), Detachment folding in the central and eastern Zagros fold belt (Iran), *J. Struct. Geol.*, *27*, 1680–1696.

Stocklin, J. (1968), Structural history and tectonics of Iran: A review, *Am. Assoc. Pet. Geol. Bull.*, *52*, 1229–1258.

Stocklin, J. (1974), Possible ancient continental margins in Iran, in *Geology of Continental Margins*, edited by C. A. Burk and C. L. Drake, pp. 873–877, Springer, New York.

Stoneley, R. (1981), The geology of the Kuh-e-Dalneshin of southern Iran, and its bearing on the evolution of southern Tethys, *J. Geol. Soc. London*, *138*, 509–526.

Talbot, C. J., and M. Alavi (1996), The past of a future syntaxis across the Zagros, in *Salt Tectonics*, edited by G. I. Alsop, D. J. Blundell, and I. Davison, *Spec. Pap. Geol. Soc. Am.*, *100*, 89–109.

Talebian, M., and J. A. Jackson (2004), A reappraisal of earthquake focal mechanisms and active shortening in the Zagros mountains of Iran, *Geophys. J. Int.*, *156*, 506–526.

Tatar, M., D. Hatzfeld, J. Martinod, A. Walpersdorf, M. Ghafori-Ashtiany, and J. Chéry (2002), The present-day deformation of the central Zagros from GPS measurements, *Geophys. Res. Lett.*, *29*(19), 1927, doi:10.1029/2002GL015427.

Tatar, M., D. Hatzfeld, and M. Ghafori-Ashtiany (2004), Tectonics of the central Zagros (Iran) deduced from microearthquakes seismicity, *Geophys. J. Int.*, *156*, 255–266.

Twiss, R. J., and J. R. Unruh (1998), Analysis of fault slip inversions: Do they constrain stress or strain rate?, *J. Geophys. Res.*, *103*, 12,205–12,222.

Vernant, P., et al. (2004), Present-day crustal deformation and plate kinematics in the Middle East constrained by GPS measurements in Iran and northern Oman, *Geophys. J. Int.*, *157*, 381–398.

Wessel, P., and W. H. F. Smith (1998), New improved version of the Generic Mapping Tools released, *Eos Trans. AGU*, *79*, 579.

Yamaji, A., S. Tomita, and M. Otsubo (2005), Bedding tilt test for paleostress analysis, *J. Struct. Geol.*, *27*, 161–170.

Yilmaz, Y., E. Yigitbas, and S. C. Gens (1993), Ophiolite and metamorphic assemblages of SE Anatolia and their significance in the geological evolution of orogenic belts, *Tectonics*, *12*, 1280–1297.

O. Lacombe, B. Meyer, and F. Mouthereau, Laboratoire de Tectonique, UMR 7072 CNRS, Université Pierre et Marie Curie, T26-25, E1, Boite 129, 4 place Jussieu, F-75252 Paris, France. (olivier.lacombe@lgs.jussieu.fr)

S. Kargar, Geological Survey of Iran, Shiraz, Iran.